

The public reporting burden for this collection of information is estimated to average 1 hour per response, including the time for reviewing instructions, searching existing data sources, gathering and maintaining the data needed, and completing and reviewing the collection of information. Send comments regarding this burden estimate or any other aspect of this collection of information, including suggestions for reducing this burden, to Washington Headquarters Services, Directorate for Information Operations and Reports, 1215 Jefferson Davis Highway, Suite 1204, Arlington VA, 22202-4302. Respondents should be aware that notwithstanding any other provision of law, no person shall be subject to any penalty for failing to comply with a collection of information if it does not display a currently valid OMB control number.  
PLEASE DO NOT RETURN YOUR FORM TO THE ABOVE ADDRESS.

1. REPORT DATE (DD-MM-YYYY) 04-08-2018	2. REPORT TYPE Final Report	3. DATES COVERED (From - To) 5-May-2015 - 4-May-2018
---	--------------------------------	---

4. TITLE AND SUBTITLE Final Report: Multiscale Modeling of Probabilistic Failure of Quasibrittle Structures Under Impact Research Topic Area: Engineering; Program Manager: Dr. Larry C. Russell, Jr.	5a. CONTRACT NUMBER W911NF-15-1-0197
	5b. GRANT NUMBER
	5c. PROGRAM ELEMENT NUMBER 611102

6. AUTHORS	5d. PROJECT NUMBER
	5e. TASK NUMBER
	5f. WORK UNIT NUMBER

7. PERFORMING ORGANIZATION NAMES AND ADDRESSES University of Minnesota - Minneapolis 450 McNamara Alumni Center 200 Oak Street SE Minneapolis, MN 55455 -2070	8. PERFORMING ORGANIZATION REPORT NUMBER
---	--

9. SPONSORING/MONITORING AGENCY NAME(S) AND ADDRESS (ES) U.S. Army Research Office P.O. Box 12211 Research Triangle Park, NC 27709-2211	10. SPONSOR/MONITOR'S ACRONYM(S) ARO
	11. SPONSOR/MONITOR'S REPORT NUMBER(S) 65374-EG-YIP.6

12. DISTRIBUTION AVAILABILITY STATEMENT Approved for public release; distribution is unlimited.
--

13. SUPPLEMENTARY NOTES The views, opinions and/or findings contained in this report are those of the author(s) and should not be construed as an official Department of the Army position, policy or decision, unless so designated by other documentation.
---

14. ABSTRACT
--------------

15. SUBJECT TERMS
-------------------

16. SECURITY CLASSIFICATION OF:			17. LIMITATION OF ABSTRACT UU	15. NUMBER OF PAGES	19a. NAME OF RESPONSIBLE PERSON Jialiang Le
a. REPORT UU	b. ABSTRACT UU	c. THIS PAGE UU			19b. TELEPHONE NUMBER 612-625-0752

# RPPR Final Report

## as of 30-Oct-2018

Agency Code:

Proposal Number: 65374EGYIP

Agreement Number: W911NF-15-1-0197

### INVESTIGATOR(S):

**Name:** Jialiang Le  
**Email:** jle@umn.edu  
**Phone Number:** 6126250752  
**Principal:** Y

Organization: **University of Minnesota - Minneapolis**

Address: 450 McNamara Alumni Center, Minneapolis, MN 554552070

Country: USA

DUNS Number: 555917996

EIN: 41-6007513

**Report Date:** 04-Jan-2018

Date Received: 04-Aug-2018

**Final Report** for Period Beginning 05-May-2015 and Ending 04-May-2018

**Title:** Multiscale Modeling of Probabilistic Failure of Quasibrittle Structures Under Impact Research Topic Area: Engineering; Program Manager: Dr. Larry C. Russell, Jr.

**Begin Performance Period:** 05-May-2015

**End Performance Period:** 04-May-2018

**Report Term:** 0-Other

Submitted By: Jialiang Le

Email: jle@umn.edu

Phone: (612) 625-0752

**Distribution Statement:** 1-Approved for public release; distribution is unlimited.

**STEM Degrees:** 0

**STEM Participants:** 1

**Major Goals:** The proposed research aims to develop a robust computational model for predicting the probabilistic fracture behavior of quasibrittle structures. The model will address the issue of spurious mesh dependence in stochastic finite element simulations, which is one of the fundamental challenges in computational modeling of quasibrittle fracture. This research will create a new scientific understanding of how the damage localization mechanism would influence the stochastic computation of quasibrittle fracture. This understanding is essential for improving the efficiency and accuracy of the computational model, which will allow us to predict the failure behavior of large-scale structures without performing full-scale experiments. Meanwhile, this model will also provide us a means to physically relate the stochastic failure response of macroscale structures to the variability of the material's microstructural properties, such as the grain size distribution and the fracture properties of grain boundaries.

This research will be anchored by a stochastic multiscale computational framework. At the macroscale, a new probabilistic crack band model will be developed to mitigate the mesh dependence of stochastic finite element simulations. The relevant parameters of this macroscopic model will be calibrated through a series of stochastic mesoscale simulations of material elements of different sizes at various strain rates. This framework will be applied to analyze the probabilistic failure behavior of quasibrittle structures under impact loading. The research will consist of the following four tasks:

Task 1 Stochastic mesoscale modeling of ceramic materials:

This task will focus on the development of a discrete element model (DEM) for ceramics, which can realistically capture the various microstructural characteristics, such as grain size distribution and grain boundary properties. To extend this DEM to stochastic analysis, the optimal linear estimation method will be applied to efficiently generate the auto-correlated random field of grain boundary properties. The proposed stochastic DEM will be used to simulate the size dependent probabilistic failure behavior of material elements at different strain rates.

Task 2 Development of a probabilistic crack band model:

A new crack band model will be developed for stochastic finite element simulations of quasi-static fracture. The model will consist of two components: 1) fracture energy regularization for the transition between damage initiation and localization; and 2) a finite weakest-link model to describe the random onset of localization band. The model will naturally involve an internal material length scale, which is essential for mitigating the mesh dependence of stochastic finite element simulations.

Task 3 Development of a theoretical model for rate-dependent failure statistics:

## RPPR Final Report as of 30-Oct-2018

To capture the strain rate effect on strength statistics, a new analytical model of probability distribution of dynamic strength of ceramics will be developed based on the concept of finite weakest-link statistics. The statistical parameters will be calibrated based on the stochastic DEM simulations. In this way, the statistics of the macroscopic dynamic strength can be related to the probabilistic failure behavior of the material at the mesoscale. This rate-dependent weakest-link model could further be incorporated into the probabilistic crack band model.

**Task 4 Investigation of mesh sensitivity in stochastic simulations of dynamic quasibrittle fracture**

The last task of the research is to investigate the mesh sensitivity in stochastic simulations of failure behavior of quasibrittle structures under impact loading. As a model system, we will simulate the split Hopkinson pressure bar (SHPB) experiments on alumina nitride specimens. The focus will be on the prediction of the dynamic tensile strength of the specimen. The simulations will include the conventional crack band model and the probabilistic crack band model. The study of the mesh sensitivity will shed light on the potential success of a new computational model that combines the probabilistic crack band model and rate-dependent weakest link model.

**Accomplishments:** Please see the attached final report of the project.

**Training Opportunities:** During the course of the project, one female PhD student was recruited to work full time on this project. One other PhD student has also worked on part of the project. In addition to PhD students, an undergraduate research assistant was recruited to work on the project. One PhD student will graduate in December 2018. The undergraduate student has graduated, and is currently pursuing a MS/PhD in my group.

The first PhD student has focused on 1) development of a theoretical model of scaling of dynamic strength distribution of quasibrittle materials, 2) model calibration using stochastic DEM simulations, and 3) stochastic simulation of the split Hopkinson bar pressure experiments.

The other PhD student has worked on the weakest-link statistical model. His focus is on the understanding of the internal length scale of the weakest-link model.

The undergraduate research assistant has assisted in performing stochastic DEM simulations of ceramic specimens of different sizes under dynamic loading.

## RPPR Final Report as of 30-Oct-2018

**Results Dissemination:** The PI has published one research monograph, which contains some work performed in this project.

Z. P. Bazant and J.-L. Le (2017) Probabilistic Mechanics of Quasibrittle Structures: Strength, Lifetime, and Size Effect, Cambridge University Press.

The research team has also published three journal papers, and another paper is currently under preparation.

J.-L. Le and J. Elias (2016) "A probabilistic crack band model for quasibrittle fracture", Journal of Applied Mechanics, ASME, 83(5), 051005 (7 pages).

J.-L. Le, Z. Xu, and J. Elias "Internal length scale of finite weakest-link model of quasibrittle fracture", J. Eng. Mech., ASCE, 144(4), 04018017 (11 pages)

J.-L. Le, J. Elias, A. Gorgogianni, J. Vievering, and J. Kveton "Rate-dependent scaling of dynamic tensile strength of brittle and quasibrittle structures", J. Appl. Mech., ASME, 85(2), 021003 (12 pages)

The PI and his students also presented these results in major conferences including the 2015 Society of Engineering Sciences Annual Meeting, the ASCE Engineering Mechanics Institute Conference in 2015-2018, the 9th International Conference on Fracture of Concrete Structures, and the 13th World Congress on Computational Mechanics. Here is the list of conference presentations:

J.-L. Le and J. Elias, "A probabilistic crack band model for quasibrittle fracture", ASCE Engineering Mechanics Institute Conference, Stanford University, June 2015.

J.-L. Le and J. Elias "A new crack band model for probabilistic analysis of quasibrittle fracture", Proceedings of IV International Conference on Computational Modeling of Fracture and Failure, Cachan, France, 2015.

J.-L. Le and J. Elias, "Mitigating mesh dependence of stochastic finite element analysis of quasibrittle fracture", ASCE Engineering Mechanics Institute Conference, Vanderbilt University, May 2016.

J.-L. Le and J. Elias, "Investigation of mesh dependency of stochastic simulations of quasibrittle fracture." Proceedings of 9th International Conference on Fracture Mechanics of Concrete and Concrete Structures, Berkeley, May 2016.

A. Gorgogianni, J. Vievering, and J.-L. Le "Rate and size effects on strength distribution of quasibrittle structures", ASCE Engineering Mechanics Institute Conference, San Diego, May 2017.

J.-L. Le and A. Gorgogianni "Rate dependent weakest-link statistical model of quasibrittle fracture", ASCE Engineering Mechanics Institute Conference, MIT, May 2018.

J.-L. Le and A. Gorgogianni, "Rate and size effects on dynamic tensile strength of quasibrittle structures", The 13th World Congress on Computational Mechanics, New York City, July 2018

**Honors and Awards:** EMI Leonardo da Vinci Award, American Society of Civil Engineers 2017  
Award citation: for important contributions to probabilistic mechanics of quasibrittle structures, scaling of their failure and consequent reliability-based structural design.

2016 Young Engineer of the Year, Minnesota Federation of Engineering, Science, and Technology Societies.

**Protocol Activity Status:**

**Technology Transfer:** Nothing to Report

### **PARTICIPANTS:**

**Participant Type:** PD/PI

**Participant:** Jialiang Le

**RPPR Final Report**  
as of 30-Oct-2018

**Person Months Worked:** 1.00

**Funding Support:**

Project Contribution:  
International Collaboration:  
International Travel:  
National Academy Member: N  
Other Collaborators:

**Participant Type:** Graduate Student (research assistant)

**Participant:** Zhifeng Xu

**Person Months Worked:** 2.00

**Funding Support:**

Project Contribution:  
International Collaboration:  
International Travel:  
National Academy Member: N  
Other Collaborators:

**Participant Type:** Graduate Student (research assistant)

**Participant:** Anna Gorgogianni

**Person Months Worked:** 10.00

**Funding Support:**

Project Contribution:  
International Collaboration:  
International Travel:  
National Academy Member: N  
Other Collaborators:

**Participant Type:** Undergraduate Student

**Participant:** Joshua Vievering

**Person Months Worked:** 1.00

**Funding Support:**

Project Contribution:  
International Collaboration:  
International Travel:  
National Academy Member: N  
Other Collaborators:

**BOOKS:**

**Publication Type:** Book

Peer Reviewed: Y **Publication Status:** 1-Published

Publication Identifier Type: ISBN

Publication Identifier: 9781107151703

Book Edition: Volume:

Publication Year: 2017

Date Received: 17-Oct-2017

Publication Location: Cambridge, UK

Publisher: Cambridge University Press

**Book Title:** Probabilistic Mechanics of Quasibrittle Structures: Strength, Lifetime, and Size Effect

**Authors:** Zdenek P. Bazant, and Jia-Liang Le

**Editor:**

Acknowledged Federal Support: Y

**CONFERENCE PAPERS:**

**RPPR Final Report**  
as of 30-Oct-2018

**Publication Type:** Conference Paper or Presentation

**Publication Status:** 1-Published

**Conference Name:** 9th International Conference on Fracture Mechanics of Concrete and Concrete Structures

Date Received: 26-Oct-2016      Conference Date: 29-May-2016      Date Published:

Conference Location: University of California, Berkeley

**Paper Title:** Investigation of Mesh Dependence of Stochastic Simulations of Quasibrittle Fracture

**Authors:** Jan Elias and Jia-Liang Le

Acknowledged Federal Support: **Y**

# **FINAL REPORT**

**on**

## **Multiscale Modeling of Probabilistic Failure of Quasibrittle Structures Under Impact**

**Project No: W911NF1510197**

**JIALIANG LE**

Department of Civil, Environmental, and Geo- Engineering  
University of Minnesota  
Minneapolis, Minnesota 55455, USA

**August 4, 2018**

## Table of Contents

List of Figures	4
Chapter 1. Problem Statement	6
Chapter 2. Probabilistic Crack Band Model	10
2.1. Introduction	10
2.2. Probabilistic modeling of damage initiation, localization and propagation	11
2.3. Numerical Examples	19
2.4. Results and Discussion	22
Chapter 3. Development of Stochastic Discrete Element Model	27
3.1. Introduction	27
3.2. Model Description	28
3.3. Simulation of Dynamic Tensile Failure of AlN Specimens	33
Chapter 4. Rate Dependent Weakest-Link Modeling of Strength Statistics	40
4.1. Introduction	40
4.2. Model Description	42
4.3. Comparison with Stochastic Discrete Element Simulations	49
Chapter 5. Mesh Dependence in Stochastic Simulations of Dynamic Quasibrittle	
Fracture	57
5.1. Introduction	57
5.2. Description of Analysis	58
5.3. Results and Discussion	60
Chapter 6. Conclusions and Future Work	65

<u>6.1. Conclusions</u>	65
<u>6.2. Future Work</u>	66
<u>References</u>	68

## List of Figures

1.1	Probabilistic analysis of failure of a uniaxial tensile bar.	7
2.1	Damage localization in one material element.	13
2.2	Determination of localization level using information of neighboring Gauss points.	14
2.3	Regularization of fracture energy based on localization parameter $\kappa_c$ .	16
2.4	Propagation of localized damage.	18
2.5	Dependence of the effective number of potential crack bands on the localization parameter $\kappa_w$ .	19
2.6	Loading configurations of three specimens: a) uniaxial tension, b) pure bending, and c) three-point bending.	20
2.7	Simulated strength distributions of three specimens with different mesh sizes.	23
2.8	Distribution of localization parameter $\kappa_w$ at the peak load.	25
2.9	Deterministic calculations of the nominal structural strengths.	25
3.1	Representation of discrete element model: a) domain discretization, and b) Voronoi body and facet.	29
3.2	Representation of discrete element model: a) domain discretization, and b) Voronoi body and facet.	33
3.3	A square specimen loaded by a prescribed strain rate.	34
3.4	Simulated average nominal stress-strain curves for different specimens sizes and strain rates.	36

3.5	Simulated damage patterns of specimens of $D = 400\mu\text{m}$ at the peak load.	37
3.6	Simulated size effect on the mean structural strength at different strain rates.	38
3.7	Simulated size effect on the standard deviation of the structural strength at different strain rates.	39
4.1	A rectangular specimen loaded by a prescribed strain rate: a) schematic of the specimen, and b) weakest-link model representation.	43
4.2	Modeling of strength distribution of one RVE: a) hierarchical model of a static RVE, and b) fiber-bundle model of a RVE under high strain-rate loading.	44
4.3	Simulated mean size effect curves of nominal strength at different strain rates and the optimum fits by the rate-dependent finite weakest-link model.	50
4.4	Strain rate effect on the RVE size.	51
4.5	Influence of strain rate on the statistical parameters of $P_1(\sigma_N)$ .	52
4.6	Simulated size effects on the standard deviation of nominal strength at different strain rates and its comparison with the rate-dependent finite weakest-link model.	54
5.1	Schematics of simulation set-up: a) input stress pulse, b) impacted specimen, and c) a typical free-end velocity profile.	59
5.2	Simulated mean dynamic strengths for different mesh sizes: a) conventional crack band model, and b) probabilistic crack band model.	61
5.3	Simulated standard deviations of dynamic strength for different mesh sizes: a) conventional crack band model, and b) probabilistic crack band model.	62
5.4	Simulated damage profile at the measurement of the pullback velocity: a) $\dot{\epsilon} = 500/\text{s}$ , b) $\dot{\epsilon} = 750/\text{s}$ , and c) $\dot{\epsilon} = 1000/\text{s}$ .	63

## CHAPTER 1

**Problem Statement**

Resistance to high velocity impact is a key design consideration for many defense structures. Due to the intrinsic stochasticity of both material microstructure and local material properties, the structural response under impact loading could exhibit a considerable degree of variability. Understanding this stochastic structural behavior is of paramount importance for the reliability-based design of defense structures. Modern defense structures are often made of advanced materials, which are brittle heterogeneous (quasibrittle) in nature. Typical examples include engineering ceramics, fiber composites, particulate reinforced composites, etc. The dynamic failure behavior of brittle and quasibrittle structures has been a major research interest for almost two decades [77, 62, 84, 61, 41, 32, 21, 16, e.g.]. Since direct experimental investigation is usually limited to certain specimen geometries and sizes, which are likely to be very different from the actual designs, there is a strong interest in developing advanced computational models to predict the response of the actual structures under various loading conditions.

Quasibrittle materials generally exhibit a strain-softening behavior, which causes damage localization in the structure. The size of the localized damage zone represents an intrinsic length scale, which has a dominant effect on the fracture behavior. It has transpired that damage localization in quasibrittle structures would lead to a major difficulty in finite element (FE) calculations known as the spurious mesh sensitivity [11, 14, 89, 8]. In conventional FE simulations without considering any length scales, damage (or smeared cracking) could localize into an arbitrarily small region which is dictated by the FE mesh size. Consequently, the simulated structural response is largely dependent on the mesh size. Such spurious mesh sensitivity is unacceptable since the physical responses cannot be influenced by the mesh discretization besides the numerical convergence error. Over

the years, various localization limiters such as crack band model [11] and nonlocal integral and gradient models [93, 89, 8], which explicitly take into account the intrinsic length scales of material fracture, have been developed to overcome the mesh sensitivity issue for FE simulations of the mean structural behavior of quasibrittle structures under quasi-static loading.

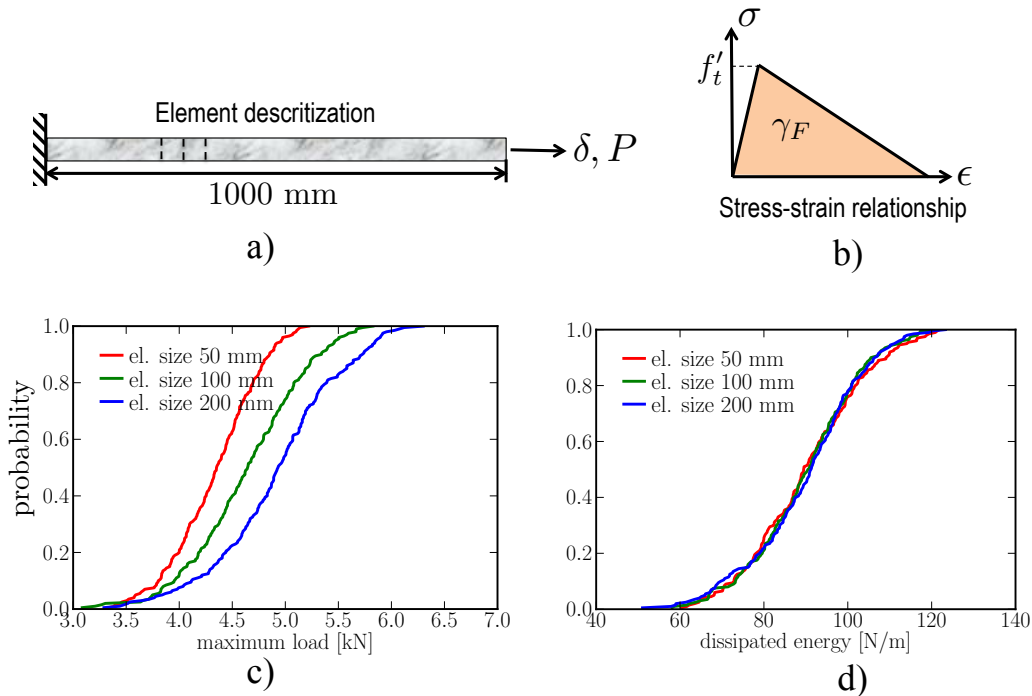


Figure 1.1. Probabilistic analysis of failure of a uniaxial tensile bar.

By contrast, though significant advances have been made in developing novel analytical and numerical models for studying quasibrittle fracture, very few studies have addressed the spurious mesh sensitivity in *stochastic FE simulations*. This spurious mesh sensitivity can be demonstrated by considering a bar under quasi-static uniaxial tension, where the bar is sub-divided into several elements along its length (Fig. 1.1a). Due to the strain-softening behavior, damage will localize into one element. If we consider that each element has a random material strength  $f_t$  and fracture energy density  $\gamma_F$ , which are statistically uncorrelated, the peak load of the bar  $P_{\max}$  is governed by the minimum strength of the element, i.e.  $P_{\max} = A_0 \min_i(f_{ti})$  ( $A_0$  = cross sectional area and  $i$  = element number). Evidently, the probability distribution of  $P_{\max}$  must be dependent on

the number of elements in the bar, which implies that the mesh size would affect the computed probabilistic structural response. The existing localization limiters, which were largely formulated within a deterministic framework, cannot adequately ensure the mesh objectivity for stochastic simulations. To demonstrate it, we calculated the cumulative distribution function (cdf) of  $P_{\max}$  by using the conventional crack band model with some commonly used assumptions: 1) the material has a linear softening stress-strain behavior (Fig. 1.1b), 2) the random material strength and fracture energy density in each element are statistically independent, and 3) the cdf of  $f_t$  for each element follows a Gauss-Weibull grafted distribution [10, 64]. Fig. 1.1c shows the computed cdfs of  $P_{\max}$  for different element sizes. It can be seen that the resulting cdf strongly depends on the element size. On the other hand, the cdf of the total energy dissipation of the bar is independent of the element size (Fig. 1.1d) since the crack band model was used here to regularize the fracture energy.

The aforementioned mesh sensitivity issue has severely hampered the prediction capacity of stochastic computational models for quasibrittle structures. The problem becomes more complicated for the case of dynamic quasibrittle fracture, since the applied strain rate is known to have a strong influence on the damage localization mechanism [14, 32]. Therefore, the regularization of mesh dependence has to take into account the strain rate effect. One way to circumvent the general mesh-dependence issue is to use a micromechanics-based model instead of the continuum smeared cracking model [3, 36, 113, 25, 61, 84, 41, 24, 32]. For instance, several recently developed micromechanical models were able to explicitly represent various microstructural features such as inhomogeneity geometry and pre-existing flaws [113, 61, 21]. These models can well capture the essential physics of damage initiation and growth. Therefore, the intrinsic length scales associated with the damage process become the natural outcome of the simulation. Nevertheless, the primary drawback of micromechanics-based models for stochastic simulations is that they require a significant amount of computational time, which sometimes makes them even prohibitive for large-size structures.

Based on the foregoing discussion, it is clear that the continuum FE models can offer an efficient means to simulate stochastic dynamic behavior of large-size structures but they generally suffer from the issue of spurious mesh sensitivity. On the other hand, micromechanics-based models are able to capture the essential physics of dynamic material fracture but the computational cost can be very high. This research aims to develop a robust computational model that can mitigate the mesh dependence issue in stochastic computation of quasibrittle fracture. The essence of the model is to combine the stochastic discrete element computational model and the macroscopic FE model through an analytical probabilistic model. The research yields the following four results: 1) a probabilistic crack band model, 2) a stochastic discrete element model, 3) a probabilistic model for the rate and size dependence of dynamic strength, and 4) mesh dependence issue in dynamic quasibrittle fracture. The subsequent chapters of this report will summarize these findings.

## CHAPTER 2

**Probabilistic Crack Band Model****2.1. Introduction**

One of the most salient features of quasibrittle materials is that they generally exhibit a strain softening stress-strain behavior after the peak strength is attained, which leads to the strain localization phenomenon. Strain localization can be broadly understood as a form of instability defined as the onset of formation of a finite size band with non-homogenous deformation while the material outside the band is subjected to a homogeneous deformation under the equilibrium condition. The constitutive localization instability has been analyzed by many researchers for materials with a plastic behavior [46, 97, 80] as well as with a damage softening behavior [94, 52]. It has been shown that the necessary condition for the onset of this localization instability at a material point can be determined by the eigenvalue analysis of the acoustic tensor, sometimes also referred to as the localization tensor.

From the viewpoint of computation, localization instability is known to cause spurious mesh sensitivity in the finite element (FE) simulations of quasibrittle fracture. This is because the strain softening behavior would cause damage to localize into a single layer of elements, and thus the energy needed to cause material damage is governed by the chosen mesh discretization. Such an unrealistic prediction can be corrected by introducing a material length scale into the model, which prevents damage localization into a zero-size element. This class of models is usually referred to as the localization limiters. The simplest localization limiter is the crack band model developed by Bažant and Oh [11], in which the post-peak portion of the stress-strain curve of the material is adjusted such that the overall fracture energy is kept constant. Though the crack band model provides a convenient way to mitigate the mesh dependence in FE simulations of quasibrittle fracture,

special care needs to be taken for the proper definition of the element size under a multi-axial stress state as well as for high-order elements [6, 56, 53]. A more sophisticated approach adopts the concept of the nonlocal continuum, where it is assumed that the constitutive behavior of a material point depends on both the local constitutive variables (e.g. inelastic strains, damage, energy dissipation) and the values of these constitutive variables in the surrounding material points [1, 5, 93, 13, 88, 87].

One common feature of the aforementioned localization limiters is that they were developed for deterministic analysis of quasibrittle fracture. Some recent research efforts have been directed towards the understanding of the effect of strain localization on the reliability analysis of quasibrittle structures due to its paramount importance for structural design [10, 64]. These studies have focused on the theoretical aspects of the probability distribution of structural strength with its associated scale effect. Even though the mathematical framework of stochastic FE simulation of structural response has reached a high degree of sophistication [103, 40, 106], there is still a lack of understanding of how the strain localization mechanism would affect the stochastic FE analysis of quasibrittle fracture.

In this part of the research, we develop a probabilistic crack band model (PCBM) for stochastic FE simulations of quasibrittle structures. This model combines the conventional crack band model and a probabilistic treatment of damage evolution.

## 2.2. Probabilistic modeling of damage initiation, localization and propagation

The essential idea of the conventional crack band model is to adjust the material's constitutive relationship in order to preserve fracture energy for localized damage. Such regularization of fracture energy is essential for mitigating the spurious mesh dependence in deterministic FE simulations of quasibrittle fracture. Inspired by this concept, we attempt to investigate how to adjust the probability distributions of the constitutive relationship in order to achieve the mesh objectivity of stochastic FE simulations.

In this study, we limit our attention to tensile damage, where the stress-strain response is characterized by three parameters, namely the elastic modulus  $E$ , the tensile strength  $f_t$

and the total energy dissipation density (i.e. area under the uniaxial stress-strain curve)  $\gamma$ . We consider that the randomness of the stress-strain relation is purely governed by the randomness of the tensile strength and the energy dissipation density. It is noted that the same assumption has been adopted by some recent studies on probabilistic analysis of quasibrittle fracture [42, 35]. Therefore, the crux of problem is to determine the probability distribution of  $f_t$  and  $\gamma$  by taking into consideration the processes of damage initiation and localization.

In the FE simulations, the constitutive behavior of each Gauss point represents the mechanical behavior of a material element. Evidently the size of this material element is determined by the finite element size. Consider this material element of size  $h_e$  subjected to an applied stress, as shown in Fig. 2.1. Upon loading, a damage band could occur in this material element. This band has a fixed width  $h_0$ , usually referred to as the crack band width, which is generally different from the material element size  $h_e$ . Previous studies have demonstrated that for quasibrittle materials the crack band width is about two to three times the maximum size of the material inhomogeneities [14, 7, 12]. This crack band width represents a characteristic length scale of the damage localization process. Meanwhile, for probabilistic analysis, the other length scale that is generally needed is the auto-correlation length  $l_a$ , which describes the spatial random field of material properties. Recent studies have shown that, for a material element of size equal to the crack band width, the material properties can be considered as statistically independent variables [12, 42, 64]. Therefore, it is expected that the auto-correlation length should be considerably smaller than the crack band width. Since the interest of this study lies in the case where the element size is larger than the crack band width, i.e.  $h_e > h_0$ , we can treat the material properties of each element as statistically independent random variables.

### 2.2.1. Determination of localization level

The fracture process of quasibrittle materials can be considered to consist of three stages, which include damage initiation, damage localization, and damage propagation. The damage initiation stage usually involves the formation of a large distributed cracking

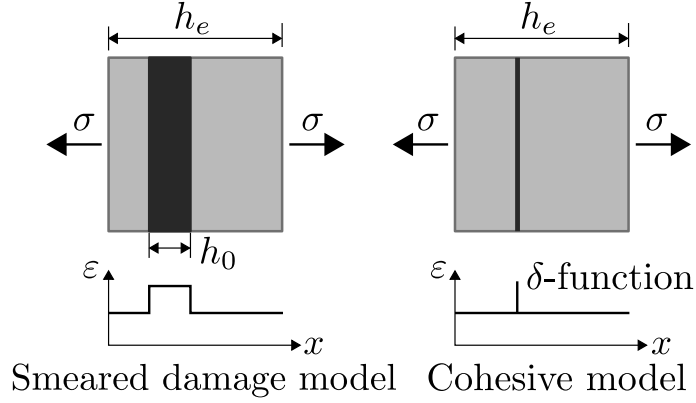


Figure 2.1. Damage localization in one material element.

zone. As the loading continues, these distributed cracks start to localize into one macro-crack, and this macro-crack further propagates with a fracture process zone attached at its tip. As will be described later, it is essential to differentiate these three stages for the probabilistic analysis of quasibrittle fracture since they have very different implications on the regularization of energy dissipation as well as on the probabilistic treatment of localized damage.

In the context of FE simulations, we first propose a parameter for each Gauss point that measures the level of localization:

$$\kappa_c = \begin{cases} \frac{1}{(n_i+n_o)} \left[ \frac{(n_i+n_o+1) \cdot \max_{k \leq n_o+n_i} (\phi_k)}{\sum_{k=0}^{n_i+n_o} \phi_k} - 1 \right], & \text{if } \phi_0 > 0 \\ 0, & \text{if } \phi_0 = 0 \end{cases} \quad (2.1)$$

where  $n_i$  = number of surrounding Gauss points within the element of interest (i.e. inner neighbors in Fig. 2.2),  $n_o$  = number of surrounding Gauss points within the neighboring elements (outer neighbors in Fig. 2.2),  $\phi_0$  = damage level of the Gauss point of interest,  $\phi_k$  = damage level of the  $k$ th surrounding Gauss points,  $k \in \{1, \dots, n_i\}$  refers to inner neighbors, and  $k \in \{n_i+1, \dots, n_i+n_o\}$  refers to outer neighbors. The damage level  $\phi$  may conveniently be defined in the context of continuum damage mechanics. For example,  $\phi$  can simply be chosen to be equal to the damage parameter if a damage constitutive model is used. The detailed definition of the damage level is not of particular importance for

Eq. 2.1 since the present definition of  $\kappa_c$  uses the damage levels in a relative sense. It is clear from Eq. 2.1 that the value of  $\kappa_c$  would increase with the level of strain localization, and the maximum possible value of  $\kappa$  would be equal to 1, which corresponds to the case where only one Gauss point exhibits damage.

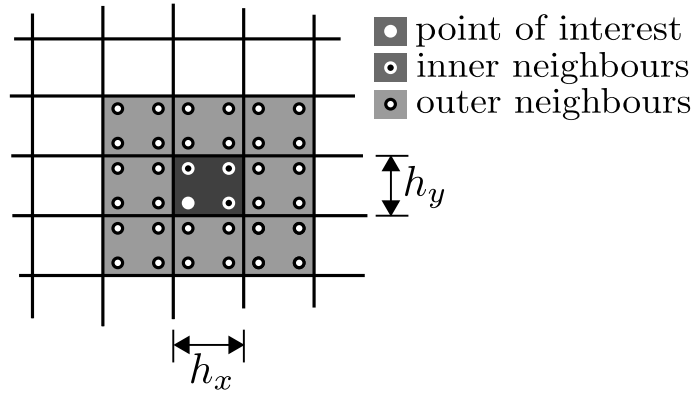


Figure 2.2. Determination of localization level using information of neighboring Gauss points.

Eq. 2.1 indicates that for each Gauss point the localization level is determined by two conditions: 1) the Gauss point itself should experience damage, and 2) the surrounding Gauss points should exhibit a pattern of strain localization. The first condition corresponds to the fact that for quasibrittle materials the localization tensor of a material point becomes singular approximately when the material tensile strength is reached, which is a necessary but not sufficient condition for determining the onset of strain localization [52]. For a finite body, the onset of localization is also influenced by the structural geometry and stress field. An explicit mathematical description of this condition is not available, and therefore in this study we use the information of the damage level of the surrounding Gauss points to determine the localization level.

In addition to the strain localization level of each Gauss point, it is also necessary to determine the localization level of the surrounding Gauss points, which is described by

$$\kappa_w = \frac{1}{n_o - 1} \left[ \frac{n_o \cdot \max_{k=n_i+1}^{n_i+n_o} \phi_k}{\sum_{k=n_i+1}^{n_i+n_o} \phi_k} - 1 \right] \quad (2.2)$$

Different from the previously defined parameter  $\kappa_c$ , the localization parameter  $\kappa_w$  only considers the surrounding Gauss points. In Section 2.3, we will show that, though  $\kappa_w$  does not indicate the strain localization of the Gauss point of interest, it provides useful information that determines the randomness of the onset of the localization band for that Gauss point. This is essential for constructing the probability distribution function of the strength of a material element. Furthermore it is noted that both localization parameters  $\kappa_c$  and  $\kappa_w$  are non-decreasing, which is similar to the irreversibility of material damage during the loading process.

### 2.2.2. Regularization of fracture energy

We first formulate the probability distribution function of the energy dissipation density based on the requirement of preservation of fracture energy for localized damage. Energy regularization is an essential concept of the conventional crack band model [11, 14], which can be demonstrated by approximating the localized damage band as a cohesive crack (Fig. 2.1). It is evident that the fracturing strain of the material element is equal to the opening of the cohesive crack divided by the material element size. Therefore, we have

$$\gamma h_e = G_f \quad (2.3)$$

where  $G_f$  = fracture energy of the material. Eq. 4.1 indicates that the stress-strain response is dependent on the material element size. Here we define a reference stress-strain response that corresponds to a material element of size equal to the crack band width  $h_0$ . We further use  $\gamma_0$  to denote the energy dissipation density for this reference stress-strain response, and clearly we have  $\gamma_0 h_0 = G_f$ .

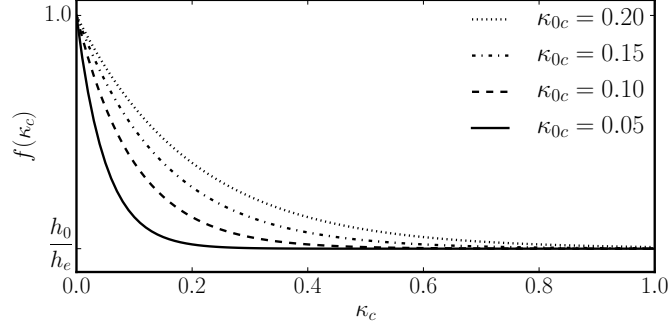


Figure 2.3. Regularization of fracture energy based on localization parameter  $\kappa_c$ .

It is clear that Eq. [4.1](#) is written by considering that localization has occurred, which does not explicitly address the transition from damage initiation to localization. At the damage initiation stage, the entire material element would suffer damage and therefore the total energy dissipation of the material should be proportional to the element size. To account for such a transition, we propose a phenomenological energy regularization equation using the localization parameter  $\kappa_c$ :

$$\gamma = \gamma_0 f(\kappa_c) \quad (2.4)$$

$$\text{where: } f(\kappa_c) = \frac{h_0}{h_e} + \left(1 - \frac{h_0}{h_e}\right) \exp\left(-\frac{\kappa_c}{\kappa_{0c}}\right) \quad (2.5)$$

Function  $f(\kappa_c)$  leads to a smooth transition of the energy dissipation density from  $\gamma_0$  to  $G_f/h_e$  as the damage localizes (Fig. [3.1](#)), and the transition is governed by the parameter  $\kappa_{0c}$ .

Following the aforementioned formulation, we can determine the cumulative distribution function (cdf) of the energy dissipation density  $\gamma$  from the probability distribution of the fracture energy

$$F_\gamma(x) = \Pr(\gamma \leq x) \quad (2.6)$$

$$= F_{G_f}[xh_0/f(\kappa_c)] \quad (2.7)$$

where  $F_\gamma(x)$  = cdf of energy dissipation density and  $F_{G_f}$  = cdf of fracture energy. Eq. [2.7](#) indicates that the probability distribution of the energy dissipation density is governed

by the localization parameter as well as the material element size relative to the crack band width. However, the functional form of  $F_\gamma(x)$  is the same as that of the cdf of the fracture energy, which remains unchanged for different element sizes.

The distribution function  $F_{G_f}$  is assumed to obey a Gaussian-Weibull grafted distribution [68], which reads

$$P_{\text{GW}}(x) = \begin{cases} 1 - \exp[-(x/s_0)^m] & (x \leq x_{gr}) \\ P_{gr} + \frac{r_f}{\delta_G \sqrt{2\pi}} \int_{\sigma_{gr}}^x e^{-(x'-\mu_G)^2/2\delta_G^2} dx' & (x > x_{gr}) \end{cases} \quad (2.8)$$

where  $m$  and  $s_0$  are the shape and scale parameters of the Weibull tail, and  $\mu_G$  and  $\delta_G$  are the mean and standard deviation of the Gaussian core if considered extended to  $-\infty$ ;  $r_f$  is a scaling parameter required to normalize the grafted cdf such that  $P_{\text{GW}}(\infty) = 1$ , and  $P_{gr} = \text{grafting probability} = (x_{gr}/s_0)^m$ . The continuity of the probability density function at the grafting point requires that  $(dP_{\text{GW}}/d\sigma_N)|_{x_{gr}^+} = (dP_{\text{GW}}/d\sigma_N)|_{x_{gr}^-}$ .

### 2.2.3. Probabilistic onset of damage localization

The foregoing analysis only considers the formation of a single damage band inside the material element. However, it is evident that there is an inherent randomness of the location of the damage band. As mentioned earlier, the eigenvalue analysis of the acoustic tensor indicates that the necessary condition for the onset of the damage band is that the tensile strength is reached [52]. Therefore, we may consider that the location of the damage band in the material element is determined by the local tensile strength. In other words, the random onset of the damage band in the material element should be reflected by the statistics of the tensile strength of the corresponding Gauss point.

Since the auto-correlation length of the random field of material strength is smaller than the crack band width, we may use the classical weakest link model to describe the cdf of the material strength for each Gauss point, i.e.

$$F_{f_t}(\sigma) = 1 - [1 - P_1(\sigma)]^{n_e} \quad (2.9)$$

where  $n_e$  = number of potential crack bands that could be formed in the material element represented by the Gauss point, and  $P_1(x)$  = cdf of the tensile strength of the material element of a size equal to the crack band width. It has been shown that  $P_1(x)$  can also be described by the Gaussian-Weibull grafted distribution function (i.e. Eq. 8) [10, 64].

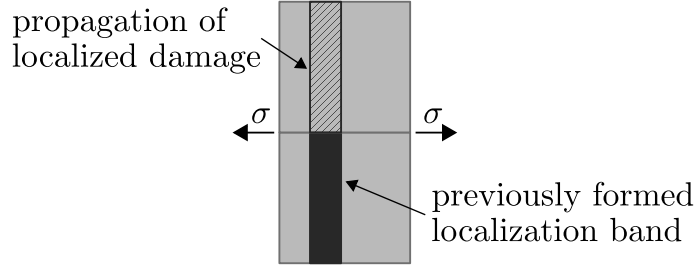


Figure 2.4. Propagation of localized damage.

To determine the number of potential crack bands  $n_e$ , it is essential to first check whether there would be a random onset of localization band in the material element. This randomness is largely governed by the strain localization level in the surrounding material elements. Consider that one surrounding material element has experienced localized damage as shown in Fig. 2.4. This indeed corresponds to the scenario of the propagation of localized damage. In such a case, the localized damage in the surrounding element would physically lead to stress concentration, which dictates the location of the localization band in the element of interest. Therefore, there would not be any randomness in the location of the localization band, which implies  $n_e = 1$ . In this study, the effect of the localization damage of the surrounding Gauss points on the weakest link model is described through an empirical function

$$n_e = 1 + \left( \frac{h_e}{h_0} - 1 \right) \exp \left( - \frac{\kappa_w}{\kappa_{0w}} \right) \quad (2.10)$$

It should be emphasized here that the strain localization mechanism has different effects on the probability distributions of energy dissipation density and material tensile strength of each Gauss point: the tensile strength is dictated by the minimum tensile strength of the material element of a size equal to crack band width whereas the energy dissipation density is directly related to the fracture energy of the material. This leads

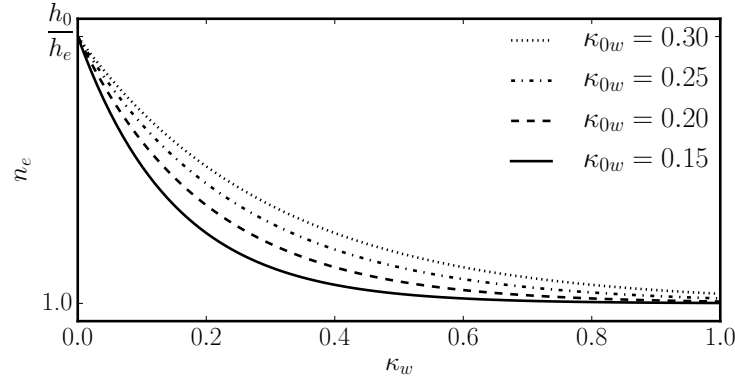


Figure 2.5. Dependence of the effective number of potential crack bands on the localization parameter  $\kappa_w$ .

to different treatments of the mesh dependence of the cdfs of tensile strength and energy dissipation density. For the present probabilistic analysis the tensile strength and fracture energy are treated as independent random variables.

### 2.3. Numerical Examples

The proposed PCBM is applied to simulate the probability distributions of the nominal strength of three concrete specimens under different loading configurations (Fig. 2.6). The nominal stresses for these three specimens are defined as the maximum principal stress based on the elastic analysis, which can be expressed as

$$\sigma_N = P/bD \text{ for uniaxial tension} \quad (2.11)$$

$$\sigma_N = 6M/bD^2 \text{ for pure bending} \quad (2.12)$$

$$\sigma_N = 3PL/2bD^2 \text{ for three-point bending} \quad (2.13)$$

where  $P, M$  = the applied load and moment,  $D$  = specimen depth,  $L$  = specimen length, and  $b$  = width of the specimen in the transverse direction. The maximum nominal stress,  $\sigma_{N,\max}$ , corresponds to the nominal stress computed for the maximum load ( $P_{\max}, M_{\max}$ ) that the specimen can sustain. For comparison purpose, two other models are also used to perform these simulations, which include 1) the crack band model (Eq. 7) without adjusting the probability distribution of tensile strength (i.e.  $n_e = 1$  for Eq. 9), which is

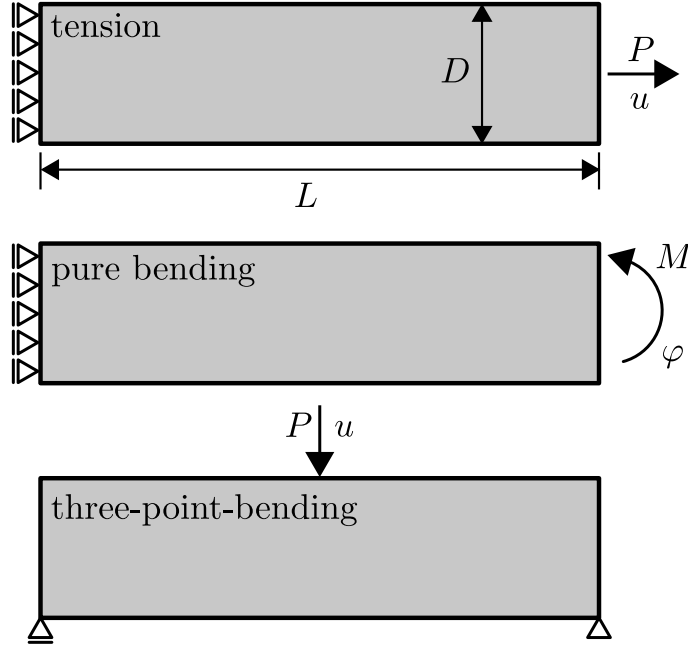


Figure 2.6. Loading configurations of three specimens: a) uniaxial tension, b) pure bending, and c) three-point bending.

denoted by CBM, and 2) the crack band model (Eq. 7) with considering the weakest link model of tensile strength regardless of the localization level (i.e.  $n_e = h_e/h_0$  for Eq. 9), which is denoted by WLM.

### 2.3.1. Constitutive model

In this analysis we consider a simple isotropic damage model even though the proposed PCBM can also be incorporated into other more sophisticated constitutive models. The present constitutive relationship can be written as

$$\boldsymbol{\sigma} = (1 - \omega)\mathbf{D} : \boldsymbol{\epsilon} \quad (2.14)$$

where  $\mathbf{D}$  =elastic stiffness tensor and  $\omega$  = damage parameter. The parameter  $\omega$  describes the damage level of the material point. Here  $\omega$  is expressed as a function of the equivalent

strain,  $\bar{\epsilon}$ , defined by [75]

$$\bar{\epsilon} = \sqrt{\sum_{I=1}^3 \langle \epsilon_I \rangle^2} \quad (2.15)$$

where  $\epsilon_{1-3}$  are principal strain values. The damage parameter is then calculated by assuming a linear softening behavior:

$$\omega = \begin{cases} 0 & \bar{\epsilon}_m \leq f_t/E \\ 1 - \frac{f_t(2\gamma - f_t\bar{\epsilon}_m)}{\bar{\epsilon}_m(2\gamma E - f_t^2)} & f_t/E < \bar{\epsilon}_m \leq 2\gamma/f_t \\ 1 & \text{otherwise} \end{cases} \quad (2.16)$$

where  $\bar{\epsilon}_m$  is the maximum value of  $\bar{\epsilon}$  that has ever been attained during the past loading history. To prevent a snap-back stress-strain behavior, the fracturing strain should not be smaller than the strain at the elastic limit, i.e.  $\gamma \leq f_t^2/2E$ , and with Eq. 4.1 we have  $h_e \leq 2G_f E/f_t^2$ . This represents an upper limit of the element size  $h_e$ . Since both  $f_t$  and  $G_f$  are random and independent variables, sampled from interval  $(0, \infty)$ , there is always some probability of having a snap-back stress-strain curve. However, this probability is extremely low for the mesh sizes used in the present study.

The present FE simulations are performed in OOFEM software [86, 85], in which the specimens are discretized using linear quadrilateral elements with four integration points. In the present model, the tensile strength and fracture energy of each Gauss point is sampled by

$$X = F_X^{-1}(\xi_X) \quad (2.17)$$

where  $X$  = sampled values of  $\gamma$  or  $f_t$ ;  $F_X(x)$  = cdfs of  $X$  defined by Eqs. 7 and 9; and  $\xi_X$  = assigned probabilities. In the numerical implementation of the model, we first generate  $\xi_X$  for each Gauss point by using a uniform distribution function over a range of  $[0, 1]$ . During the simulation, these probability values are used to compute the corresponding tensile strength and fracture energy in every solution step. The essential feature of the present model is that the damage localization level evolves during the loading process and this leads to the change in the sampling distribution functions. Consequently, the values of the sampled tensile strength and fracture energy would change over the transition from

damage initiation to localization. In the calculation, the element size  $h_e$  is measured along the direction of the maximum positive principal strain, which aligns with the direction of the crack band [14]. For each simulation step, the values of the localization parameters  $\kappa_c$  and  $\kappa_w$  are set to be their maximum values that have ever been reached during the past loading history, i.e.  $\kappa_i(t_0) = \max_{t \leq t_0} [\kappa_i(t)]$  ( $i = c, w$ ).

### 2.3.2. Description of Analysis

The present simulations are performed by assuming a 2D plane stress condition. The specimen has a depth of  $D = 0.5$  m and a length of  $L = 4$  m. The large span-to-depth ratio ensures that the beam would failure predominantly in tension even in the case of three-point bending. The beams are loaded by either a prescribed displacement or a prescribed rotation as shown in Fig. 2.6. To represent a typical concrete material, the following material parameters are used in the analysis: elastic modulus  $E = 30$  GPa, Poisson's ratio  $\nu = 0.2$ , mean tensile strength  $\bar{f}_t = 3$  MPa, and mean fracture energy  $\bar{G}_f = 80$  J/m<sup>2</sup>. For the probability distributions of tensile strength and fracture energy of a material element of the crack band size, we set the coefficient variation CoV = 0.15, the grafting distribution  $P_{gr} = 10^{-3}$ , and the Weibull modulus  $m = 26$ . The simulations consider three different mesh sizes, i.e.  $(h_x, h_y) = (50, 50)$  mm,  $(100, 50)$  mm, and  $(200, 50)$  mm, where  $h_x, h_y$  denote the width and depth of the element, respectively. The crack band width  $h_0$  is set to be 50 mm, which is about two to three times the normal aggregate size of concrete.

The model parameters  $\kappa_{0c}$  and  $\kappa_{0w}$  are determined by minimizing the differences in the probability distributions of the nominal strength simulated by using different mesh sizes for all three loading cases. This minimization yields  $\kappa_{0c} = 0.190$  and  $\kappa_{0w} = 0.283$ .

## 2.4. Results and Discussion

Fig. 2.7 presents the probability distributions of the nominal strength of three beams simulated by the aforementioned three methods. Each of these strength distributions are obtained from 1000 realizations. The simulation results for the reference element size

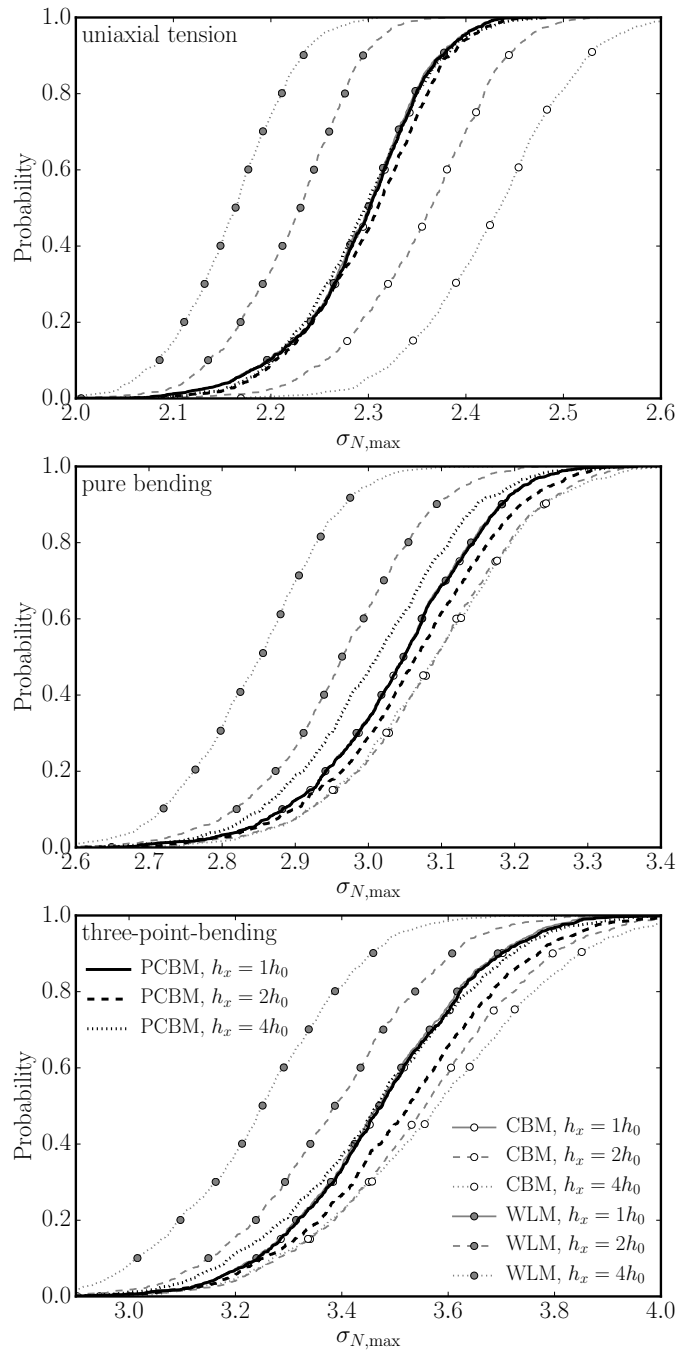


Figure 2.7. Simulated strength distributions of three specimens with different mesh sizes.

$h_x = h_0$  are used as the reference solution. For the reference size, all three methods yield the same result. It is seen that, as we use a larger element size, the CBM overestimates the structural strength for a given failure probability. Because the CBM does not take into account the potential randomness of the onset of the localization band, it overpredicts the strength distribution of the material element. On the other hand, the WLM applies the weakest link model of material strength regardless of the localization level. As the specimen attains its peak load, there is some amount of propagation of localized damage, which indicates that the weakest link model should vanish. Consequently, it is seen that the WLM underestimates the strength distribution of the beam as the element size increases.

The results show that the PCBM can effectively mitigate the mesh dependence of the simulated strength distribution. Based on the present formulation, the regularization of mesh dependence is achieved through the probabilistic treatment of damage localization (Eq. 10). Furthermore, it is essential to consider the effect of the localization level of the surrounding elements on the random onset of the localization in a single material element. It is interesting to note that for the uniaxial tension the results of PCBM and WLM exhibit a large difference but this is not the case for the other two loading scenarios. This could be explained by analyzing the spatial distribution of the parameter  $\kappa_w$  at the peak load shown as Fig. 2.8. It is clear that for both three-point bending and pure bending cases the tensile damage side of the specimen exhibits relatively high values of  $\kappa_w$ , which indicates that the PCBM is close to the CBM. By contrast, for the uniaxial tension specimen, the values of  $\kappa_w$  are more spread and therefore the difference between the PCBM and CBM is more pronounced.

Meanwhile, it is also worthwhile to comment on the importance of Eq. 5, which regularizes the fracture energy for the transition between damage initiation and localization. In the conventional crack band model [11], the fracture energy is preserved in all cases, i.e.  $\kappa_{0c} = 0$ . This is sufficient for scenarios in which distributed cracking is absent. An obvious case is structures with a pre-existing crack. For a general case in which distributed cracking transitions to localized cracking, the regularization of fracture energy of

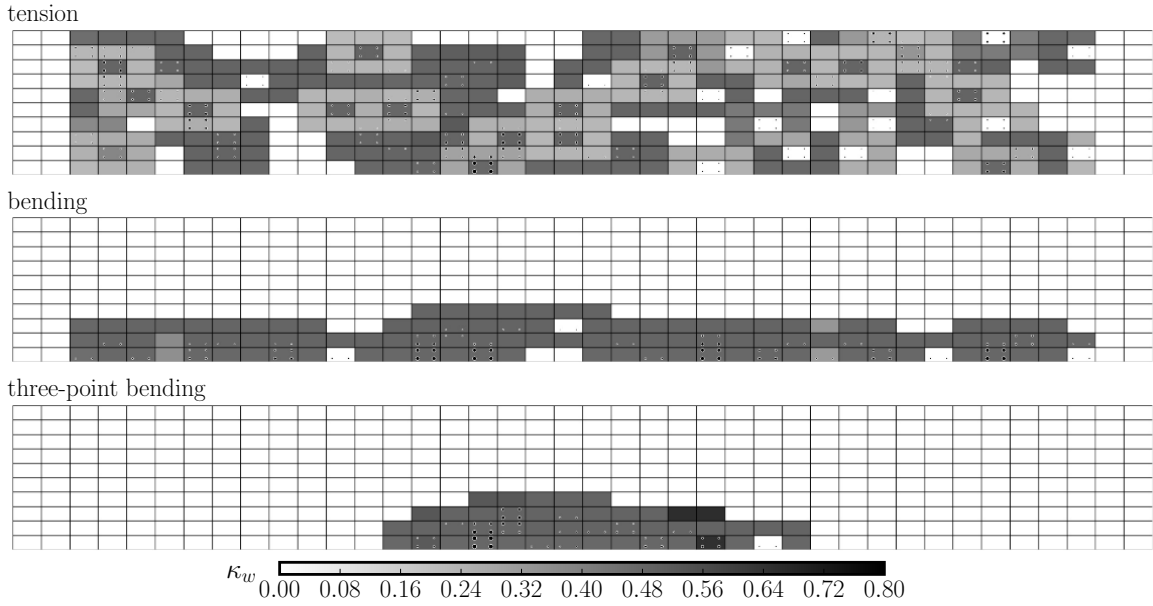


Figure 2.8. Distribution of localization parameter  $\kappa_w$  at the peak load.

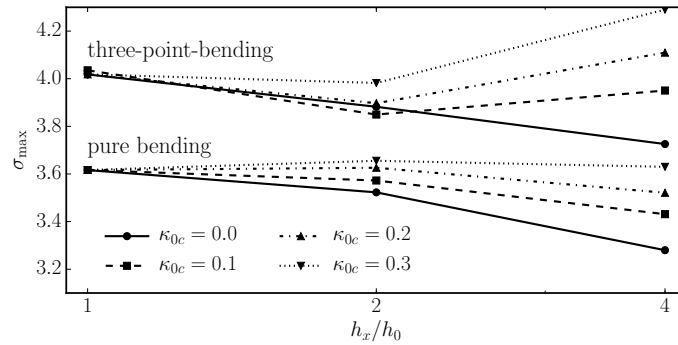


Figure 2.9. Deterministic calculations of the nominal structural strengths.

a Gauss point should be tied to the damage localization pattern in its neighborhood. To demonstrate this point, we perform deterministic calculations of the nominal strengths of beams under pure bending and three-point bending by using the present crack band model for different values of  $\kappa_{0c}$ . The calculations use the mean values of tensile strength

and fracture energy ( $f_t = \bar{f}_t = 3 \text{ MPa}$ ,  $G_f = \bar{G}_f = 80 \text{ J/m}^2$ ). Fig. 2.9 shows the results of these deterministic calculations by using different mesh sizes. It can be seen that for these two cases the conventional crack band model ( $\kappa_{0c} = 0$ ) exhibits some degree of mesh dependence. By introducing a finite value of  $\kappa_{0c}$ , such mesh dependence for deterministic calculations is seen to be reduced.

All three structures considered in the present simulations have a smooth boundary and exhibit damage initiation, localization and propagation during the loading process. If we consider specimens with a pre-existing crack, the PCBM would be the same as the CBM because the pre-existing crack has dictated the location of the damage band inside the first element at the crack tip. Furthermore, as soon as the crack-tip element reaches its strength limit, the fracture energy regularization (Eq. 5) would essentially reduce to the conventional crack band model, i.e.  $\gamma = \gamma_0 h_0 / h_c$ .

It should also be emphasized that the present study is limited to the case where the element size is larger than the crack band width. For cases where the element size is chosen to be smaller than the crack band width, the auto-correlation length scale must be introduced. The auto-correlated random fields can effectively be generated by using the spectral method [106, 35]. Further investigation is needed to explore how to efficiently incorporate the damage localization mechanism (e.g. crack band width) into these auto-correlated random fields for stochastic FE simulations.

## CHAPTER 3

**Development of Stochastic Discrete Element Model****3.1. Introduction**

In the previous chapter, we present the newly developed probabilistic crack band model and demonstrate that it can effectively mitigate the spurious mesh sensitivity in stochastic computation of quasibrittle fracture under static loading. The model is hinged on the weakest-link statistical model for strength of a material element, which physically captures the random onset of the localization band inside one finite element. The model is limited to the quasi-static loading case, in which the strain rate effect is not considered. Meanwhile, as a macroscopic continuum model, its link with the microstructural features of the material has not been established. In the second part of the research, we develop a stochastic discrete element computational model that captures the essential failure mechanisms at the mesoscale under both static and dynamic loading, and the predicted response is then used to develop a new rate-dependent weakest-link statistical model, which will be described in the next chapter.

The most realistic approach to softening damage in brittle heterogeneous materials is the discrete models in the form of either lattice or particle models. The discrete lattice model was first proposed by Hrennikoff [48] to solve elasticity problems, and was later developed for both 2D and 3D simulations of quasibrittle fracture [116, 15, 101, 54, 55, 26, 27]. The discrete particle model was originated from the so-called distinct element model developed for simulation of the behavior of particulate materials such as cohesionless soils and rock masses [22, 23]. The model was further extended to concrete materials [116], in which the material domain is discretized by a set of rigid polyhedral elements connected by nonlinear springs of zero length [58, 19, 18]. All these discrete models involve some characteristic length scale (e.g. particle size or lattice size), which acts as a

localization limiter regularizing the energy dissipation in the fracture process. In particle discrete models, the particles could either represent the actual material inhomogeneities (e.g. aggregates in concrete materials) or simply be used as an efficient means to introduce a length scale to the model [54, 55].

Over the last decade, significant advances have been made towards a realistic discrete model for various concrete materials including both conventional concrete [73, 26, 27] and fiber-reinforced concrete [99, 100]. The discrete element models have also been extended to rate-dependent failure of concrete [105]. One attractive feature of discrete models is that they provide an explicit representation of the heterogeneities of the material, which makes them well suited to handle the random size distribution of the material heterogeneities.

### 3.2. Model Description

Motivated by recent success in discrete modeling of dynamic fracture [32, 39, 104, 24, 49, 50], we develop a new stochastic discrete element model. In this model, the specimen is represented by a set of interconnected discrete rigid bodies. A set of nuclei is first randomly placed in the domain, where the mutual distance of two adjacent nuclei is controlled to be approximately equal to the grain size  $l_{\min}$  of the material. Once these nuclei are created, the Voronoi tessellation is used to discretize the domain (Fig. 3.1a). The location of the  $i$ th nuclei is denoted by  $\mathbf{x}_i$ . Each nucleus has three translational and three rotational degrees of freedom. Due to the imposition of the length scale  $l_{\min}$ , each Voronoi body can be considered to represent a material grain. The contact surface (henceforth referred to as facet) between the bodies represents the grain boundary (Fig. 3.1b). The overall nonlinear macroscopic behavior of the material is determined by the mesoscale constitutive behavior of the facets.

In this study, the formulation of the constitutive behavior of the facet follows the lattice discrete particle model (LDPM), which was originally developed for concrete materials [26, 27, 28, 29, 30, 2]. Since this study focuses primarily on macroscopic tensile failure, we adopt a simplified version of the LDPM model, which is briefly summarized here. The detailed description of the model can be found in [34].

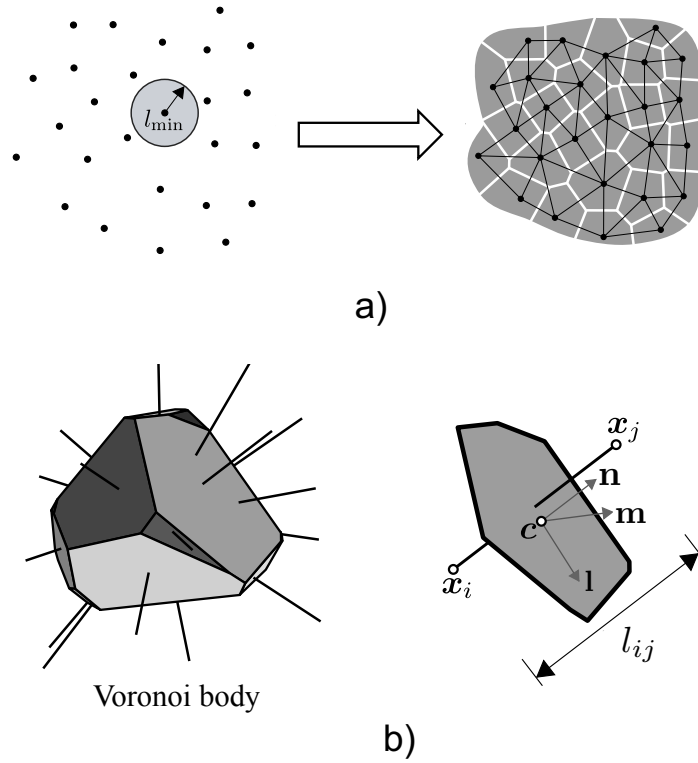


Figure 3.1. Representation of discrete element model: a) domain discretization, and b) Voronoi body and facet.

The relative motion of two adjacent Voronoi bodies directly results in displacement jumps on the facet. For two adjacent bodies  $i$  and  $j$ , the displacement jump vector  $\Delta_{ij}$  on their common facet can be calculated as [28, 34]

$$\Delta_{ij} = \mathbf{A}_j \cdot \begin{pmatrix} \mathbf{u}_j \\ \boldsymbol{\theta}_j \end{pmatrix} - \mathbf{A}_i \cdot \begin{pmatrix} \mathbf{u}_i \\ \boldsymbol{\theta}_i \end{pmatrix} \quad (3.1)$$

where  $\mathbf{u}_k, \boldsymbol{\theta}_k$  ( $k = i, j$ ) = displacement and rotation vectors of nucleus of body  $k$ , and  $\mathbf{A}_k$  ( $k = i, j$ ) = transformation matrices, which can be written as

$$\mathbf{A}_k = \begin{pmatrix} 1 & 0 & 0 & 0 & x_3^c - x_3^k & x_2^k - x_2^c \\ 0 & 1 & 0 & x_3^k - x_3^c & 0 & x_1^k - x_1^c \\ 0 & 0 & 1 & x_2^c - x_2^k & x_1^k - x_1^c & 0 \end{pmatrix} \quad (3.2)$$

where  $x_1^c, x_2^c, x_3^c$  = coordinates of the facet centroid, and  $x_1^k, x_2^k, x_3^k$  = coordinates of the nucleus of body  $k$ .

The components of the strain vector can be calculated as  $e_n = \mathbf{n} \cdot \Delta_{ij}/l_{ij}$ ,  $e_l = \mathbf{l} \cdot \Delta_{ij}/l_{ij}$ ,  $e_m = \mathbf{m} \cdot \Delta_{ij}/l_{ij}$ , where  $\Delta_{ij}$  = displacement jump vector,  $l_{ij}$  = distance between the nuclei of bodies, and  $\mathbf{n}, \mathbf{l}, \mathbf{m}$  = unit vectors in the normal and two orthogonal tangential directions, respectively. The corresponding traction vector transmitted over the facet can then be related to the strain vector by using continuum damage mechanics, i.e.

$$\begin{pmatrix} t_n \\ t_l \\ t_m \end{pmatrix} = E_0(1 - \omega) \begin{pmatrix} e_n \\ \alpha e_l \\ \alpha e_m \end{pmatrix} \quad (3.3)$$

where  $E_0$  = elastic stiffness,  $\omega$  = damage parameter, and  $t_n, t_l, t_m$  = tractions in the directions of  $\mathbf{n}, \mathbf{l}$  and  $\mathbf{m}$ , respectively. The damage parameter is expressed in terms of the equivalent stress and strain, i.e.

$$\omega = 1 - \frac{s_{\text{eq}}}{E_0 e_{\text{eq}}} \quad (3.4)$$

$$s_{\text{eq}} = f_{\text{eq}} \exp\left(\frac{K}{f_{\text{eq}}}\left\langle\chi - \frac{f_{\text{eq}}}{E_0}\right\rangle\right); \quad e_{\text{eq}} = \sqrt{e_n^2 + \alpha(e_m^2 + e_l^2)} \quad (3.5)$$

For tension and shear dominated loading, the equivalent strength  $f_{\text{eq}}$  can be defined as [28, 34]

$$f_{\text{eq}} = f_t \left[ \frac{(\eta^2 + \mu^2) \sin \psi - \sqrt{(\eta^2 - \mu^2)^2 \sin^2 \psi + 4\alpha\eta^2 \cos^2 \psi}}{2\mu^2 \sin^2 \psi - 2\alpha \cos^2 \psi} \right] \quad (3.6)$$

where  $f_t$  = tensile strength,  $f_s$  = shear strength,  $\psi = \tan^{-1} \left[ e_n / \sqrt{\alpha(e_m^2 + e_l^2)} \right]$ ,  $\eta = f_s / f_t$ , and  $\mu$  = constant. The history variable  $\chi$  is expressed as

$$\chi = \begin{cases} e_{\text{eq}} \psi / \psi_0 + e_{\text{max}} (1 - \psi / \psi_0) & \psi_0 \leq \psi < 0 \\ e_{\text{max}} & \psi \geq 0 \end{cases} \quad (3.7)$$

where  $e_{\text{max}} = \sqrt{\max(e_n^2) + \alpha \max(e_m^2 + e_l^2)}$ , in which the maxima is calculated for the entire loading history, and  $\psi_0 = -\arctan(\zeta\sqrt{\alpha})$ . For the present numerical simulations, the facets mainly experience tensile-shear damage. Therefore, it is not necessary to cover the full scenario of compressive damage.

Finally, parameter  $K$  represents the initial slope of the nonlinear branch of the constitutive law [28], which is given by

$$K = -K_t \left[ 1 - \left( \frac{\psi - \pi/2}{\psi_0 - \pi/2} \right)^{n_t} \right]; \quad n_t = \frac{\ln [K_t / (K_t - K_s)]}{\ln (1 - 2\psi_0 / \pi)} \quad (3.8)$$

where  $K_t, K_s$  are the values of  $K$  for pure tensile and shear loading, respectively.  $K_t$  and  $K_s$  are expressed as

$$K_t = \frac{2E_0}{l_t/l_{ij} - 1} \quad K_s = \frac{2\alpha E_0}{l_s/l_{ij} - 1} \quad (3.9)$$

where  $l_t = E_0 G_t / f_t^2$ ,  $l_s = E_0 G_s / f_s^2$ , and  $G_t, G_s =$  mode I and II fracture energies. It should be pointed out that Eq. 3.9 involves two material length scales  $l_t$  and  $l_s$  so that the energy expended for the fracture of a unit area of facet is independent of the distance between the nuclei.

It is worthwhile to mention that the present constitutive model itself is rate-independent, and therefore the rate effect on macroscopic behavior of the specimen is largely due to inertia and its influence on the interaction of facet failures. Such a modeling approach has been adopted in several previous discrete simulations of dynamic fracture of ceramic materials [114, 32, 61, 59], which were able to capture the rate dependent failure behavior reasonably well. Meanwhile, it has also been shown that the rate dependence of the constitutive behavior plays a secondary role in the overall failure behavior under a high strain-rate condition [82, 81], which is of interest to the present study.

The aforementioned constitutive model contains the following parameters: 1) elastic modulus  $E_0$  in the normal direction, 2) tangential to normal stiffness ratio  $\alpha$ , 3) mesoscopic tensile and shear strengths  $f_t, f_s$ , 5) mesoscopic mode I and II fracture energies  $G_t, G_s$ , and 6) constants  $\mu$  and  $\zeta$ . It is well known that the properties of quasibrittle materials usually exhibit a considerable degree of spatial variability. For studying the failure behavior, the most relevant parameters are strengths and fracture energies [42]. In this study, we characterize the spatial random distribution of mesoscopic strengths and fracture energies

by assigning a single random field  $h(\mathbf{x})$ :

$$f_t(\mathbf{x}) = \bar{f}_t h(\mathbf{x}); \quad f_s(\mathbf{x}) = \bar{f}_s h(\mathbf{x}) \quad (3.10)$$

$$G_t(\mathbf{x}) = \bar{G}_t [h(\mathbf{x})]^2; \quad G_s(\mathbf{x}) = \bar{G}_s [h(\mathbf{x})]^2 \quad (3.11)$$

Eqs. [3.10](#) and [3.11](#) imply that, on each facet, the material length scales  $l_t$  and  $l_s$  are deterministic constants. The underlying probability distribution function governing the random field  $h(\mathbf{x})$  follows the Gauss-Weibull grafted distribution (Eq. [4.2a](#) and b) with a mean value equal to one. The spatial autocorrelation of the field  $h(\mathbf{x})$  is characterized by a Gaussian function, i.e.

$$R(\delta x) = \exp[-(\delta x/l_a)^2] \quad (3.12)$$

where  $\delta x = |\mathbf{x} - \mathbf{x}'|$  and  $l_a =$  autocorrelation length. The generation of the random field  $h(\mathbf{x})$  consists of three steps [35](#): 1) a standard Gaussian random field  $\hat{h}(\mathbf{x})$  is generated on a regular square grid with a spacing of  $l_a/4$ , 2) the value of  $\hat{h}(\mathbf{x})$  on each facet is determined by using the optimal linear estimation method [70](#), and 3) the standard Gaussian field generated on the facets is converted to the Gauss-Weibull random field  $h(\mathbf{x})$  by using the isoprobabilistic transformation. Fig. [3.2](#) presents a typical realization of the random field  $h(\mathbf{x})$ .

The aforementioned computational model is numerically implemented with the implicit Newmark method [78](#), [4](#). The equation of motion is solved incrementally in an implicit scheme, which is unconditionally stable. The mass matrix is constructed by using the full inertia tensor of Voronoi bodies. The moment of inertia of these polyhedral bodies are calculated by dividing them into tetrahedra [107](#). Though a stable numerical solution scheme is chosen, a small time step is needed to capture the dynamic failure of the facet. For each simulation case, several trial simulations are performed to determine a desirable time step, which yields a consistent result.

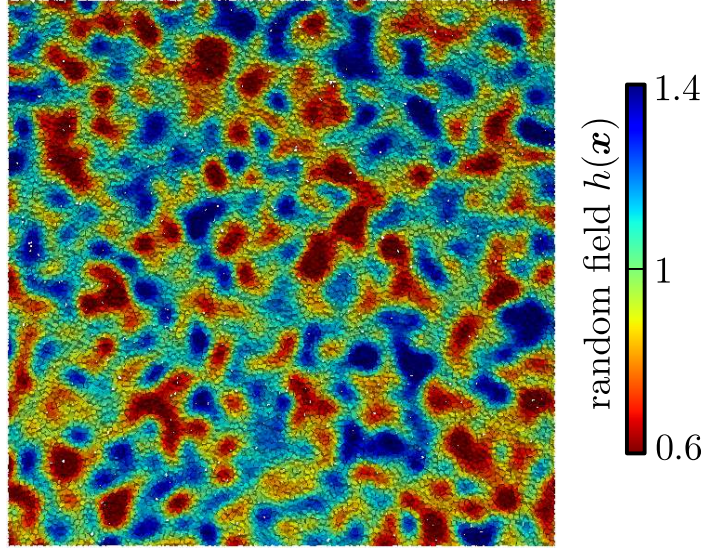


Figure 3.2. Representation of discrete element model: a) domain discretization, and b) Voronoi body and facet.

### 3.3. Simulation of Dynamic Tensile Failure of AlN Specimens

The aforementioned stochastic computational model is applied to simulate the dynamic tensile failure of aluminum nitride (AlN) specimens. In the simulations, we consider square specimens of different in-plane sizes  $D = L = 50, 100, 200, 400, 800 \mu\text{m}$  (Fig. 3.4), whereas the out-of-plane thickness is set constant  $b = 10 \mu\text{m}$ . The average in-plane grain size  $l_{\min}$  of AlN material is taken as  $6 \mu\text{m}$  [32]. Each specimen is subject to a constant strain-rate loading, which is applied by imposing a non-uniform velocity field described as  $v_{x_1} = x_1 \dot{\epsilon}$  ( $x_1$  denotes the horizontal position of each nucleus). In order to investigate the rate-dependent behavior, we consider a wide range of applied strain rates, i.e.  $\dot{\epsilon} = 1, 1000, 2500, 5000, 7500, 10^4, 3 \times 10^4, 5 \times 10^4, 10^5, 2 \times 10^5/\text{s}$ .

We choose the following mesoscale material parameters for AlN:  $E_0 = 530 \text{ GPa}$ ,  $\alpha = 0.17$ ,  $\bar{f}_t = 150 \text{ MPa}$ ,  $\bar{f}_s = 3\bar{f}_t$ ,  $\bar{G}_t = 2 \text{ Jm}^{-2}$ ,  $\bar{G}_s = 16\bar{G}_t$ ,  $\mu = 0.2$ , and  $\zeta = 0.95$ . The elastic parameters ( $E_0$  and  $\alpha$ ) are determined to match the macroscopic elastic response of AlN reported in [32]. The inelastic mesoscale material parameters are chosen so that the model

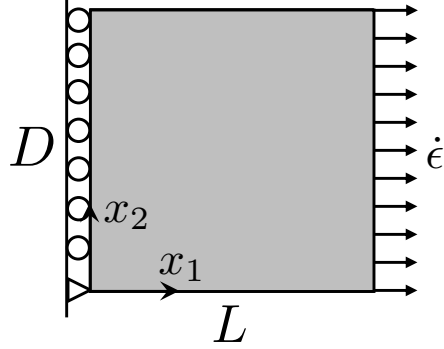


Figure 3.3. A square specimen loaded by a prescribed strain rate.

predicts the quasi-static tensile strength of a  $50 \mu\text{m}$  square AlN specimens being about 120 MPa, which is similar to the published results [32]. It is admitted that mixed-mode loading scenarios will be needed to better calibrate the coupling between tensile and shear damage. However, such a detailed calibration procedure is not necessary for the present purpose. For the random field  $h(\mathbf{x})$ , we consider that it has an autocorrelation length  $l_a$  of  $24 \mu\text{m}$ , and the underlying Gauss-Weibull distribution function has a mean value of one, a coefficient of variation of 20%, a Weibull modulus of 30 and a grafting probability of  $5 \times 10^{-4}$ .

For each specimen size and strain rate, about 70 realizations of different random fields  $h(\mathbf{x})$  and mesostructures are used to determine the mean and variance of the peak load capacity of the specimen. As mentioned earlier, the peak load capacity of the specimen is expressed in terms of the nominal strength, which in this case is equal to the maximum value of the nominal stress  $\sigma_a$  along  $x_1$ -direction (Fig. 3.4). For the present discrete system, we first calculate the fabric stress tensor of a single Voronoi body  $k$  as [96, 51]

$$\bar{\boldsymbol{\sigma}}^k = \frac{1}{V_k} \sum_{p=1}^{n_k} \mathbf{t}^p \otimes (\mathbf{x}^{cp} - \mathbf{x}^k) A_p \quad (3.13)$$

where  $V_k$  = volume of the  $k$ th body,  $n_k$  = number of facets of the body,  $\mathbf{t}^p$  = traction vector on the  $p$ th facet expressed in the global coordinate system,  $\mathbf{x}^{cp}$  = position vector of the centroid of the  $p$ th facet,  $\mathbf{x}^k$  = position vector of the nucleus of the body, and  $A_p$  = surface area of the  $p$ th facet. The nominal stress  $\sigma_a$  can then be calculated as a volume

average of the fabric stress components in the  $x_1$ -direction, i.e.:

$$\sigma_a = \frac{1}{V} \sum_{k=1}^N V_k \bar{\sigma}_{11}^k \quad (3.14)$$

where  $V$  = volume of the specimen, and  $N$  = number of Voronoi bodies in the specimen.

Based on the simulations, we obtain a set of random responses of the relationship between the nominal stress  $\sigma_a$  and the average strain  $\epsilon_a$ , where  $\epsilon_a = u/D$  and  $u$  = displacement measured at the free edge of the specimen. Fig. 3.4 presents the simulated average  $\sigma_a$ - $\epsilon_a$  curves for all specimen sizes and strain rates. It can be seen that, for a given specimen size, the average nominal strength  $\bar{\sigma}_N$ , which is the maximum value of the average nominal stress, increases with the applied strain rate. This rate enhancement is primarily due to the inertia effect. Meanwhile, we also observe that, as the strain rate increases, the post-peak softening behavior becomes less pronounced, which indicates that the specimen exhibits a more ductile behavior. This rate dependence can directly be observed from the simulated damage pattern at the peak load. As a demonstration, Fig. 3.5 shows the damage patterns of specimens of  $D = 400 \mu\text{m}$  at the peak load for different applied strain rates. It is seen that, for a given specimen size, the damage is fairly localized at low strain rates while the specimen exhibits a diffused damage pattern as the strain rate increases.

It should be pointed out that the aforementioned brittle-to-ductile transition is based on the current simulation set-up with the prescribed initial velocity field. Recent computational studies of ceramics and concrete specimens with the same set-up showed similar rate-dependent failure patterns [32, 39]. Several experiments on the rate-dependent behavior of concrete also showed the tensile stress-strain curve exhibits a more gentle post-peak softening behavior at high strain rates [43, 110]. However, there is experimental evidence showing that the compressive stress-strain response of brittle composites and ceramics could become more brittle at higher strain rates [72, 17, 57]. The set-ups of these experiments are different from the present simulations. We may expect that the rate dependence of failure behavior of quasibrittle materials could depend strongly on the specimen geometry and test set-up. This is consistent with the well accepted fact that,

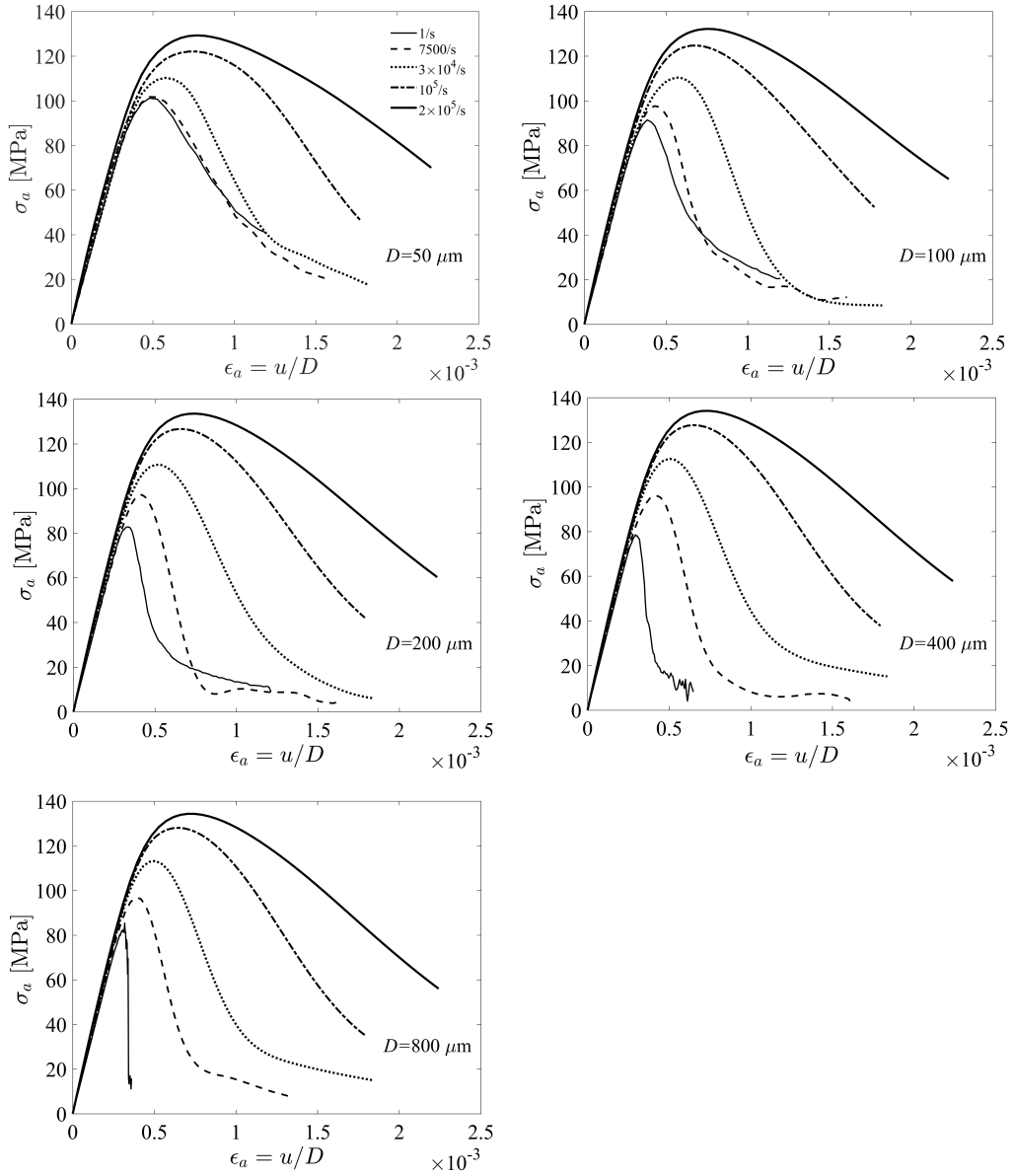


Figure 3.4. Simulated average nominal stress-strain curves for different specimen sizes and strain rates.

for quasibrittle structures, brittleness is influenced not only by the material properties, but also by the structure geometry and loading configuration [14, 7, 9].

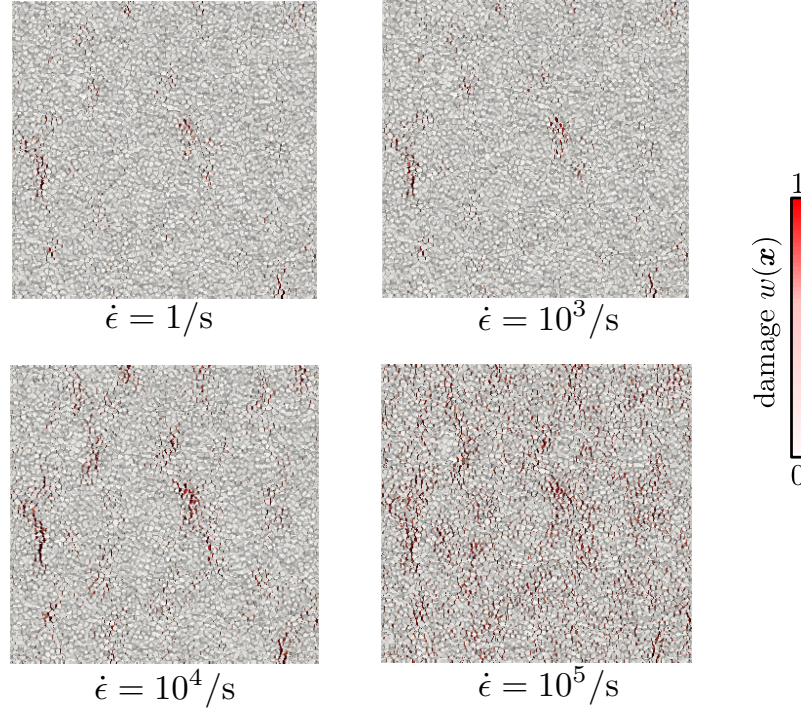


Figure 3.5. Simulated damage patterns of specimens of  $D = 400\mu\text{m}$  at the peak load.

We can also compare the simulated post-peak responses of specimens of different sizes for a given strain rate. It is seen that, at low strain rates, the slope of the post-peak softening curve becomes much steeper as the specimen size increases. This implies that the specimen experiences a more brittle failure as the specimen size increases. Such a size dependent failure behavior at low strain rates has been well documented for many quasibrittle materials, such as concrete, rock, composites, ceramics, etc. [14, 7]. As the strain rate increases, the size dependence of the post-peak behavior starts to diminish. This is consistent with the present simulation results, which show that, at high strain rates, all the specimens considered in this study exhibit a diffused cracking pattern.

The foregoing discussion reveals qualitatively the combined rate and size effects on the failure behavior of the simulated specimens. The quantitative description of these effects can be best presented in terms of the size effect on the statistics of the nominal strength.

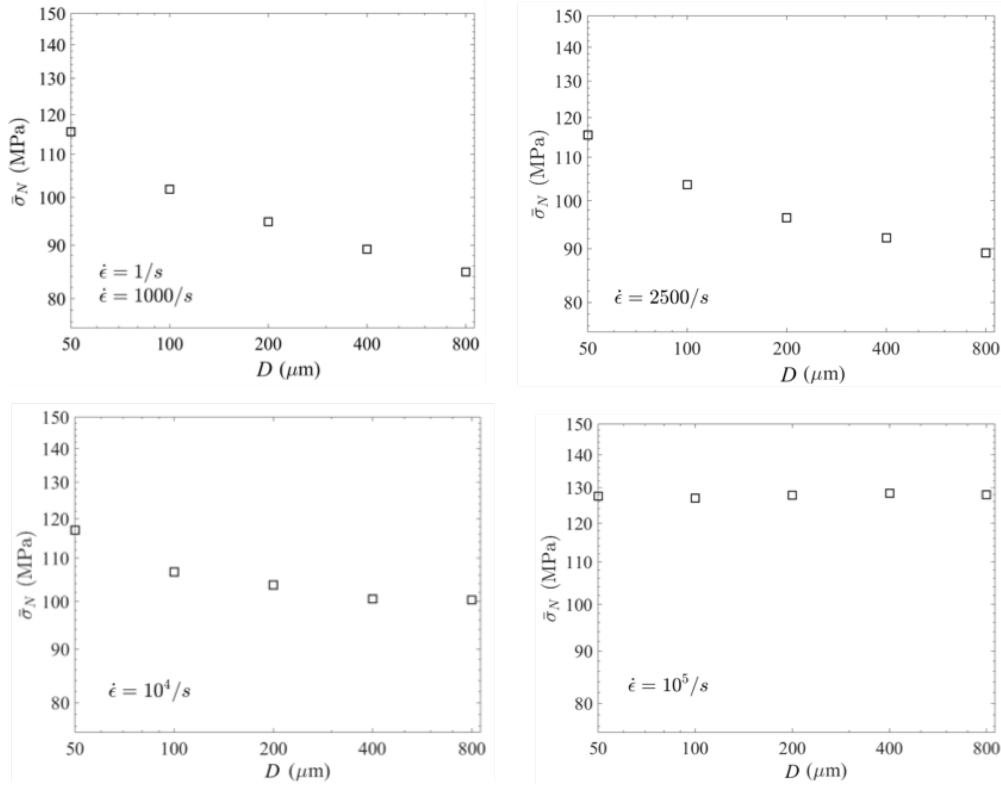


Figure 3.6. Simulated size effect on the mean structural strength at different strain rates.

Figs. 3.6 and 3.7 present the size effect curves of both the mean and standard deviation of the structural strength at different applied strain rates. The salient feature is that the mean size effect diminishes as the strain rate increases. At high strain rates, the entire specimen is occupied by diffused cracking as the peak load is reached. In this case, there is no characteristic length governing the nominal strength. Since the failure is ductile (or quasi-plastic), the size effect on the nominal strength must be absent [14, 7]. As the strain rate decreases, the damage pattern transitions from diffused cracking to localized cracking. The size of the localized damage zone represents a characteristic length scale, which leads to a non-power law form of the mean size effect curve.

Interestingly, it is observed from Fig. 3.7 that, compared to the rate effect on the mean strength, the rate effect on the standard deviation shows an opposite trend. As the

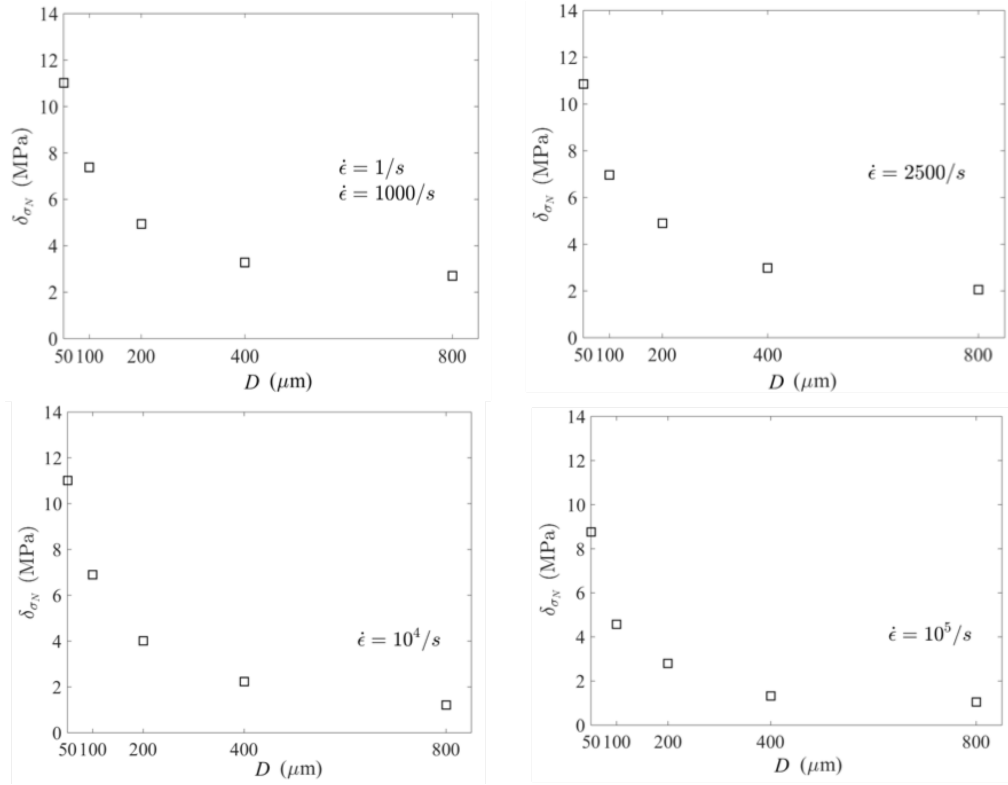


Figure 3.7. Simulated size effect on the standard deviation of the structural strength at different strain rates.

strain rate increases, the size effect on the standard deviation becomes more pronounced. Such a trend can also be explained by the strain rate effect on the damage mechanism. As discussed earlier, the damage of the specimen transitions from a localized pattern to a diffused pattern with an increasing strain rate. This implies that, for a given strain rate, the strength of the specimen can be considered as an average of the random strengths of all material elements in the specimen. Therefore, as the specimen size increases, more elements are contributing to the structural strength. Based on the Central Limit Theorem, the mean strength will approach a constant while the standard deviation of the structural strength will decrease with the specimen size.

## CHAPTER 4

**Rate Dependent Weakest-Link Modeling of Strength Statistics****4.1. Introduction**

The simulation results presented in Chapter 4 clearly indicate that the strength statistics of quasibrittle structures is strongly dependent on the structure size and applied strain rate. This finding has important implications for the stochastic finite element (FE) simulation of dynamic quasibrittle fracture. If we consider that each Gauss point represents a material element, whose size is related to the mesh size, the present model indicates that the input probability distribution of tensile strength of each Gauss point would depend on both the strain rate and mesh size. In Chapter 2, we have demonstrated that, for quasi-static loading, the influence of the mesh size on the input probability distribution of tensile strength must be taken into account in order to mitigate the mesh sensitivity in stochastic FE simulations of tensile fracture of quasibrittle structures [66].

It is evident that the simulated rate and size effects on the strength statistics has to be incorporated into the macroscopic FE simulations. Direct coupling between the stochastic discrete element model and the macroscopic FE model is not a trivial task, which still has several unsolved issues such as handling the macroscopic damage localization phenomenon, modeling the propagation of stochasticity across different scales, excessive computational time. To circumvent this difficulty, we develop an analytical strength statistical model, which is able to take into account the combined rate and size effects on the strength statistics. The model can be calibrated by the mesoscale discrete element simulations, and be incorporated into the constitutive relation for the macroscopic FE simulations. In this way, the analytical model would provide a link between the variability of mesoscale structural properties and the probability distribution of the macroscopic tensile strength.

The strength statistics of quasibrittle structures has been studied for decades. The Weibull distribution is the most widely used probabilistic model for characterizing the strength statistics of brittle structures. This probability distribution function was first derived mathematically as a type of extreme value statistics [38, 37], which describes the probability distribution of the minimum value of an infinitely large pool of independent and identically distributed random variables. Weibull independently proposed this distribution function through extensive histogram testing of strengths of many materials including Portland cement, porcelain, wood, and cotton [111, 112].

The Weibull strength distribution is based on the assumption that the structure can be statistically modeled as a chain of an infinite number of independent material elements, i.e. the infinite weakest-link model. The model physically implies that the failure of the structure is primarily governed by the damage localization mechanism and the size of the damage localization zone is negligibly small in comparison with the overall structure size. The assumption of Weibull distribution can be justified for brittle structures, in which the characteristic structure size is much larger than the size of material inhomogeneities and the location of failure point is intrinsically random due to the spatial variability of material strength.

Recent interests have been directed to structures made of quasibrittle materials, which are brittle heterogeneous in nature [12, 64, 63, 9]. As mentioned in previous chapters, the salient feature of quasibrittle structures is that the size of material inhomogeneities is not negligible compared to the characteristic structure size. As a consequence, the size of the damage localization zone represents an essential length scale governing the structural failure. Due to the existence of the non-negligible size of the damage zone, the infinite weakest-link model becomes inapplicable to quasibrittle structures. This is evidenced by the fact that the measured strength distributions of specimens made of quasibrittle materials, such as concrete, asphalt mixtures, engineering and dental ceramics, and composites, consistently deviate from the Weibull distribution [12, 10, 64, 65, 9].

In view of the inadequacy of the classical Weibull distribution for quasibrittle structures, a finite weakest-link model has recently been developed [12, 10, 64, 9]. This model

involves an essential length scale that corresponds to the size of the material representative volume element (RVE). The model was shown to be able to provide optimum fitting of the measured strength statistics of many types of quasibrittle structures [64, 65, 9]. Nevertheless, the existing finite weakest-link model is developed for the case of quasi-static loading, where the strain rate effect is absent. Therefore, it is unable to predict the rate and size dependence of the strength statistics presented in Chapter 3.

In this part of the research, we develop a rate-dependent weakest-link model for the strength statistics of quasibrittle structures. The model captures in a statistical sense the rate effect on the damage mechanism. We compare the model with the simulation results of the stochastic discrete element model (Figs. 3.6 and 3.7).

## 4.2. Model Description

Consider a set of geometrically similar rectangular quasibrittle specimens, which are loaded under displacement control with a prescribed strain rate (Fig. 4.1a). We define the nominal tensile strength,  $\sigma_N$ , as the maximum average stress that the specimen can sustain. The dependence of the mean nominal tensile strength  $\bar{\sigma}_N$  on the specimen size  $D$  arises from two sources: 1) energetic size effect due to the nonlinear softening material behavior, and 2) statistical size effect due to the spatial variability of material strength, fracture energy, and microstructure. Previous studies have shown that the small and intermediate- size regimes of this type of size effect can be captured by nonlinear deterministic models, such as the cohesive crack model, crack band model and nonlocal models, whereas the large-size regime can be described by using the Weibull statistics [7].

In a series of recent studies, it was shown that this size effect can alternatively be explained by a finite weakest-link model, which is anchored by a statistical description of structural failure [12, 64, 9]. In this model, the structure is statistically modeled as a chain of material representative volume elements (RVEs), which is often referred to as the weakest-link model (Fig. 4.1b). This model implies that the structure will fail under controlled loads once one RVE is fully damaged. In other words, in the present context the RVE is taken as the smallest material element whose failure triggers the failure of the entire structure, which is different from the RVE definition used in the classical

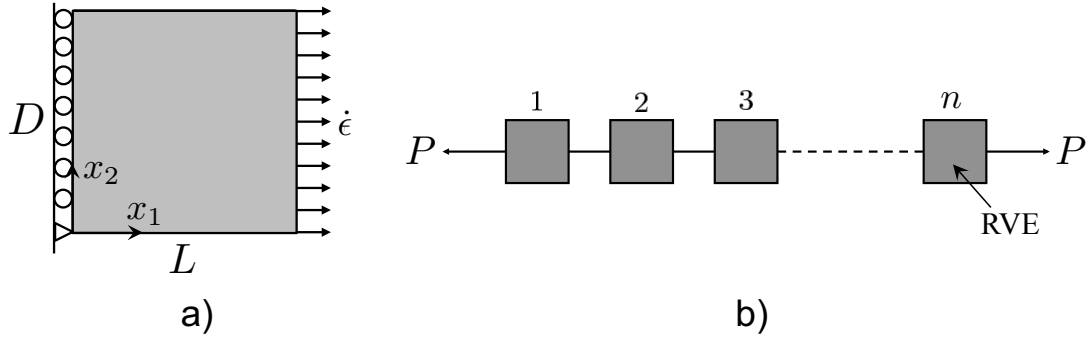


Figure 4.1. A rectangular specimen loaded by a prescribed strain rate: a) schematic of the specimen, and b) weakest-link model representation.

homogenization theory, e.g. [47, 45]. It should be emphasized that the weakest-link model is a statistical representation of the damage localization mechanism, which is a fundamental failure mechanism of quasibrittle fracture. Meanwhile, it is noted that this model is designed solely for the purpose of calculating the statistics of the structural strength, but not for determining the overall load-displacement response of the structure.

By considering that the RVE size is larger than the autocorrelation length of the random strength field [9, 42], the strength distribution of the specimen under a constant strain rate  $\dot{\epsilon}$  can be written as

$$P_f(\sigma_N, \dot{\epsilon}) = 1 - [1 - P_1(\sigma_N, \dot{\epsilon})] [1 - P_1(\sigma_N, \dot{\epsilon})]^{(n(\dot{\epsilon})-1)} \quad (4.1)$$

where  $P_1(\sigma_N, \dot{\epsilon}) =$  strength distribution of either one RVE or the entire specimen, whichever has a smaller size,  $n(\dot{\epsilon}) = A/[l_0(\dot{\epsilon})]^2$ ,  $A = DL =$  area of the specimen,  $\langle x \rangle = \max(x, 0) =$  Macaulay bracket, and  $l_0(\dot{\epsilon}) =$  RVE size, which is a function of the strain rate. Eq. 4.1 is written in a two-dimensional setting since it is reasonable to consider that the material damage occupies throughout the thickness of the specimen.

Several recent studies [32, 39] have investigated the dynamic tensile fracture behavior of ceramic and concrete materials by considering specimens similar to that depicted in Fig. 4.1a. These simulation results consistently showed that, with an increasing strain rate, the damage pattern becomes more diffusive. Therefore, we expect that the RVE size will increase with the applied strain rate. For a given specimen size, an increase in

the applied strain rate could possibly make the RVE larger than the specimen size, i.e.  $n(\dot{\epsilon}) < 1$ . In this case, Eq. 4.1 reduces to  $P_f(\sigma_N, \dot{\epsilon}) = P_1(\sigma_N, \dot{\epsilon})$ . In other words,  $P_1(\sigma_N, \dot{\epsilon})$  becomes the strength distribution of the entire specimen. This implies that the weakest-link representation of structural failure vanishes since there is no damage localization in the specimen.

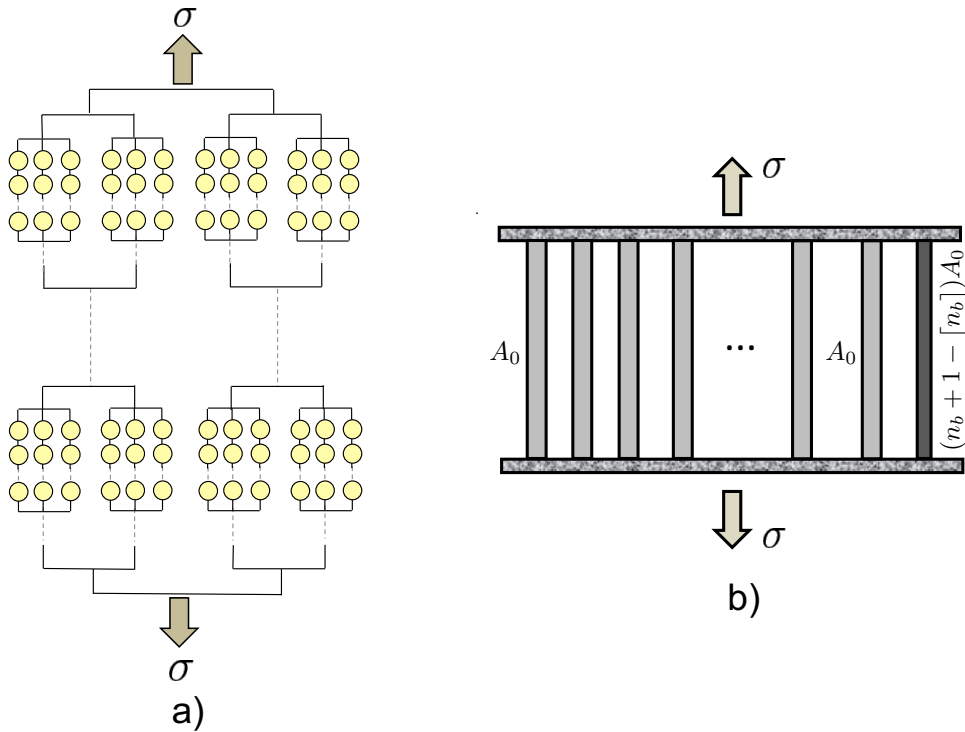


Figure 4.2. Modeling of strength distribution of one RVE: a) hierarchical model of a static RVE, and b) fiber-bundle model of a RVE under high strain-rate loading.

Based on Eq. 4.1, it is clear that the essential step is to formulate the probability distribution function  $P_1(\sigma_N, \dot{\epsilon})$ . In a series of recent studies on statistics of static strength [12, 64, 9, 10], it was shown that the RVE can be statistically modeled by a hierarchical model, which consists of a combination of bundles and chains (Fig. 4.2a). This hierarchical model represents the damage localization and load redistribution mechanisms at different

material scales. The basic element in the model represents a nanoscale structure, either an atomic lattice or a disordered system of nano-particles. The failure statistics of the nanoscale structure can be derived by using the transition rate theory and atomistic fracture mechanics [64, 9, 10]. Based on the hierarchical model, it was shown that the probability distribution of the static strength of the RVE can be approximated by a Gaussian distribution onto which a Weibull tail (or, equivalently, a power-law tail) is grafted at a fairly low probability. Mathematically, it can be written as

$$P_1(\sigma_N) = \begin{cases} 1 - \exp(-\langle \sigma_N/s_0 \rangle^{m_0}) \approx \langle \sigma_N/s_0 \rangle^{m_0} & (\sigma_N \leq \sigma_{\text{gr}}^0) & (4.2a) \\ P_{\text{gr}}^0 + \frac{r_{f0}}{\delta_{G0}\sqrt{2\pi}} \int_{\sigma_{\text{gr}}^0}^{\sigma_N} e^{-(x-\mu_{G0})^2/2\delta_{G0}^2} dx & (\sigma_N > \sigma_{\text{gr}}^0) & (4.2b) \end{cases}$$

where  $m_0$  and  $s_0$  are the Weibull modulus and the scale parameter of the Weibull tail, respectively, and  $\mu_{G0}$  and  $\delta_{G0}$  are the mean and standard deviation of the Gaussian core if considered extended to  $-\infty$ ;  $r_{f0}$  is a scaling parameter required to normalize the grafted distribution such that  $P_1(\infty) = 1$ ,  $\sigma_{\text{gr}}^0 =$  grafting stress, and  $P_{\text{gr}}^0 = (\sigma_{\text{gr}}^0/s_0)^m =$  grafting probability. Here the subscript and superscript “0” denote the case of quasi-static loading. The continuity of the probability density function (pdf) at the grafting point requires that  $[dP_1/d\sigma_N]_{\sigma_{\text{gr}}^0+} = [dP_1/d\sigma_N]_{\sigma_{\text{gr}}^0-}$ . Therefore, we need four of these parameters to define the grafted distribution of RVE strength.

To incorporate the strain rate effect into the distribution function  $P_1(\sigma_N, \dot{\epsilon})$ , we first denote the size of the RVE under quasi-static loading as  $l_{0s}$ , and henceforth we refer to the material element of size  $l_{0s}$  as the static RVE. We can then define a parameter  $n_b$ , which is equal to the equivalent number of static RVEs in the RVE or in the entire specimen, whichever is smaller, under high strain-rate loading, i.e.

$$n_b(\dot{\epsilon}) = \min[n(\dot{\epsilon}), 1] \left[ \frac{l_0(\dot{\epsilon})}{l_{0s}} \right]^2 \quad (4.3)$$

In this study, we propose to determine the distribution function  $P_1(\sigma_N, \dot{\epsilon})$  for dynamic strength by using a fiber-bundle model (Fig. 4.2b), in which each element (also called “fiber”) represents one static RVE. Since  $n_b$  may not be an integer, we consider the bundle contains  $\lceil n_b \rceil$  fibers, where  $\lceil n_b \rceil =$  the least integer that is greater than or equal to  $n_b$ .

In this bundle,  $\lceil n_b \rceil - 1$  fibers have the same cross-sectional area  $A_0$ , and the remaining fiber has a cross-sectional area of  $(n_b + 1 - \lceil n_b \rceil)A_0$ . The fiber-bundle model statistically represents the damage redistribution mechanism of the RVE under high strain rates (or of the entire specimen if  $n(\dot{\epsilon}) < 1$ ). Since the autocorrelation length of the random strength field is considered to be smaller than the size of the static RVE, the random strength of each individual fiber can be treated as statistically independent.

The investigation of the strength statistics of fiber bundles has a long history. The pioneering work of Daniels [31] dealt with brittle bundles with an equal load sharing rule, and a recursive equation was derived for the corresponding strength statistics. A considerable amount of efforts were subsequently devoted to studying brittle fiber bundles with other types of phenomenological loading sharing rules [91, 92]. A more realistic approach is to determine the load sharing rule from the mechanical behavior of the fiber. Here we consider a fiber bundle, which consists  $\lceil n_b \rceil$  fibers connected by two rigid plates (Fig. 4.2b). As discussed earlier, each fiber represents a static RVE. For quasibrittle materials, the mechanical behavior of the static RVE will exhibit some degree of strain-softening. On the other hand, we also note that the static RVE should behave in a quasi-plastic manner since it contains only a few material inhomogeneities [12]. This quasi-plastic failure behavior is also manifested by the dominant Gaussian distribution of RVE strength as indicated by Eq. 4.2b [12, 64, 9]. Therefore, the stress-strain curve of the static RVE must have a gentle softening behavior even under quasi-static loading. As the applied strain rate increases, the static RVE would experience more diffusive micro-cracking, which alleviates the degree of strain softening [43, 110, 32, 39].

The strength statistics of fiber bundles with a strain-softening behavior has recently been studied [64, 9, 98]. The calculation of the strength statistics requires the detailed information of the softening behavior of the static RVE, which is generally not available. Based on the aforementioned discussion on the quasi-plastic behavior of the static RVE, it is reasonable to approximate that the RVE exhibits a plastic stress-strain behavior, which greatly simplifies the analysis. In this case, the total strength of the bundle is essentially

equal to a weighted sum of the random strengths of fibers, i.e.

$$\sigma_N^b = \frac{1}{n_b} \left[ \sum_{i=1}^{\lceil n_b \rceil - 1} \sigma_i + (n_b + 1 - \lceil n_b \rceil) \sigma_{\lceil n_b \rceil} \right] \quad (4.4)$$

where  $\sigma_i$  ( $i = 1, \dots, \lceil n_b \rceil$ ) are the random strengths of the individual fibers. The strength distribution of each fiber is predominantly Gaussian with a very short power-law tail (Eqs. 4.2a and 4.2b). Previous studies have shown that, for such a strength distribution of fibers, the strength distribution of the bundle will also contain a power-law tail, and meanwhile the core of the strength distribution of the bundle is Gaussian [12]. Therefore, it is clear that the previously proposed grafted distribution function (Eqs. 4.2a and 4.2b) provides the correct functional form for the strength distribution function  $P_1(\sigma_N, \dot{\epsilon})$  though the values of the statistical parameters must now depend on the applied strain rate.

As mentioned earlier, the grafted strength distribution function can be determined by any four statistical parameters in Eqs. 4.2a and 4.2b. In this study, we incorporate the strain rate dependence into the strength distribution function  $P_1(\sigma_N, \dot{\epsilon})$  through the following four parameters:

- The Weibull modulus  $m$  measures the exponent of the power-law tail of the bundle. By using the series expansion method, it was shown that the power-law exponent of the bundle is equal to the sum of the power-law exponents of the tail distributions of the individual fibers [12]. In fact, this property also holds for brittle and softening bundles, where the randomness of the stress-strain curve of the fibers is described by an affine transformation [64, 9, 98]. Meanwhile, the strain rate may also affect the Weibull modulus of the static RVE itself, which is described by an empirical function  $f(\dot{\epsilon})$  to be determined later. Following these considerations, we can express the Weibull modulus of the distribution function  $P_1(\sigma_N, \dot{\epsilon})$  as

$$m(\dot{\epsilon}) = m_0 f(\dot{\epsilon}) \lceil n_b(\dot{\epsilon}) \rceil \quad (4.5)$$

- The grafting probability  $P_{gr}$  determines the extent of the power-law tail. Previous studies have shown that, as the number of fibers increases, the power-law tail of

the strength distribution of the bundle shortens at the rate of  $(P_{gr,f}/[n_b])^{[n_b]}$  ( $P_{gr,f}$  is the grafting probability of strength distribution of an individual fiber) [12]. By further considering the potential influence of the strain rate on the grafting probability of the static RVE, the rate-dependent grafting probability is written as

$$P_{gr}(\dot{\epsilon}) \approx [P_{gr}^0 g(\dot{\epsilon}) / [n_b(\dot{\epsilon})]]^{[n_b(\dot{\epsilon})]} \quad (4.6)$$

where the term  $P_{gr}^0 g(\dot{\epsilon})$  describes the rate-dependent grafting probability of the static RVE. Based on Eq. 4.6, it is clear that the Weibull tail of the RVE strength is shortened drastically as  $n_b$  increases. This means that, when the strain rate is sufficiently high, Eq. 4.5 becomes practically unimportant.

- Parameter  $\mu_G$  is approximately equal to the mean strength of the plastic bundle. The power-law tail of the strength distribution of each fiber is too short to influence the mean behavior. Based on the statistics of the weighted sum of independent Gaussian variables (Eq. 4.4), it is clear that  $\mu_G$  is equal to the mean strength of each fiber, which leads to the following expression

$$\mu_G(\dot{\epsilon}) = \mu_{G0} p(\dot{\epsilon}) \quad (4.7)$$

where  $p(\dot{\epsilon})$  is the rate enhancement function of the mean strength of the static RVE.

- Parameter  $\delta_G$  measures the standard deviation of the bundle strength since the power-law tail of the distribution function has a minimal influence on the second moment of statistics. The statistics of the weighted sum of independent Gaussian variables gives

$$\delta_G(\dot{\epsilon}) = \frac{\delta_{G0} q(\dot{\epsilon})}{n_b} [ [n_b] - 1 + (n_b + 1 - [n_b])^2 ]^{1/2} \quad (4.8)$$

where function  $q(\dot{\epsilon})$  describes the influence of the strain rate on the standard deviation of the strength of the static RVE.

By substituting Eqs. 4.5-4.8 into the grafted distribution function (Eqs. 4.2a and 4.2b), we obtain the rate-dependent strength distribution function  $P_1(\sigma_N, \dot{\epsilon})$ . Based on

the finite weakest-link model (Eq. 4.1), we can then calculate the mean dynamic strength of the specimen as

$$\bar{\sigma}_N(\dot{\epsilon}) = \int_0^1 \sigma_N dP_f(\sigma_N, \dot{\epsilon}) = \int_0^\infty [1 - P_1(\sigma_N, \dot{\epsilon})] [1 - P_1(\sigma_N, \dot{\epsilon})]^{n(\dot{\epsilon})-1} d\sigma_N \quad (4.9)$$

Meanwhile, the model also yields the rate-dependent second moment of strength statistics. For instance, the standard deviation of the dynamic strength can be calculated as

$$\delta_{\sigma_N}(\dot{\epsilon}) = \sqrt{\int_0^1 \sigma_N^2 dP_f(\sigma_N, \dot{\epsilon}) - [\bar{\sigma}_N(\dot{\epsilon})]^2} \quad (4.10)$$

By considering specimens of different sizes, we can determine the effect of specimen size on the statistics of dynamic strength. Together with the aforementioned rate dependence, Eqs. 4.9 and 4.10 describe the combined size and rate effects on the first and second moments of the statistics of nominal tensile strength of the specimen.

### 4.3. Comparison with Stochastic Discrete Element Simulations

We now use the rate-dependent finite weakest-link model (Eq. 4.9) to compare with the rate and size effects on the mean and standard deviation of the structural strength predicted by the stochastic discrete element model (Figs. 3.6 and 3.6). It is seen from Fig. 4.3 that the model can match well the simulation results for all strain rates. Based on this fitting, we determine the rate effect on the RVE size and the strength distribution of the static RVE. Fig. 4.4 presents the effect of strain rate on the RVE size. It is clear that the RVE size  $l_0$  increases with the strain rate. It is seen that the RVE size is almost a constant for the relatively low strain rates, and increases mildly for a range of intermediate strain rates  $3 \times 10^4 - 5 \times 10^4$ /s. When the strain rate exceeds  $5 \times 10^4$ /s, the RVE size increases significantly with the strain rate. In fact, for the high strain-rate regime studied here, the analysis indicates that all the specimens are smaller than the RVE. Therefore, the actual RVE size is not known. At high strain rates, the RVE can be a purely mathematical concept if the specimen does not exhibit damage localization. In this case, we may set  $l_0(\dot{\epsilon})$  to be a very large number. However, introducing the concept of the RVE for the present theoretical framework is essential because it captures the rate

dependence of the failure statistics, which transitions from a weakest-link model signifying a damage localization mechanism to a fiber-bundle model representing a diffused damage mechanism as the strain rate increases.

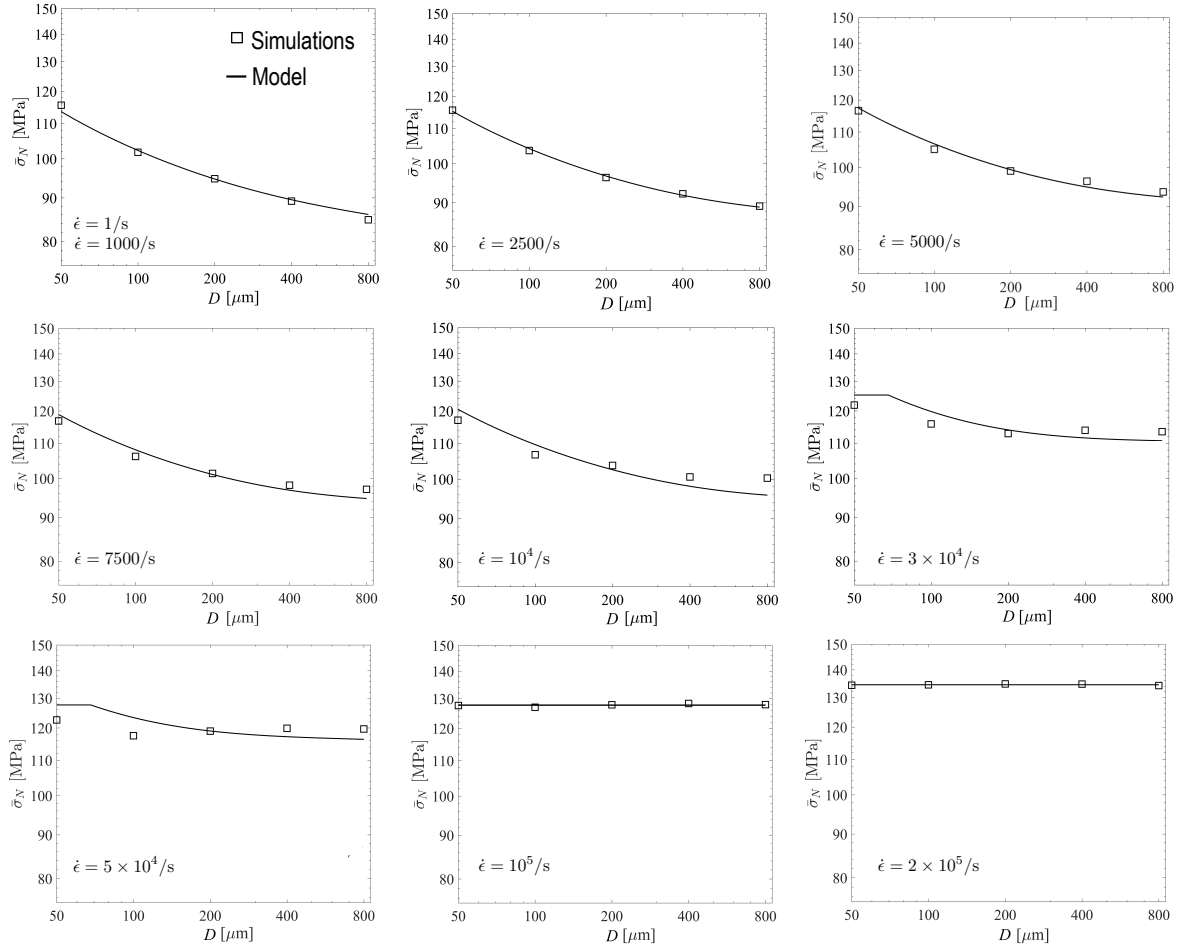


Figure 4.3. Simulated mean size effect curves of nominal strength at different strain rates and the optimum fits by the rate-dependent finite weakest-link model.

It is clear that the concept of the RVE is central to the present weakest-link model. Within the framework of weakest-link statistics, the RVE is a mathematical concept. In a recent study [67], it has been shown that the RVE size can be best determined from the optimum fitting of the mean size curve of nominal structural strength, and a relationship

between the RVE size and basic material length scales (the Irwin characteristic length and crack band width) was established for the case of quasi-static loading. Based on the results of this recent study, we expect that the RVE size will increase with the average grain size. Meanwhile, the RVE size will also increase with an increase in the fracture energies of the grain boundary. This implies that the RVE size is dependent on the loading configuration. For example, if the applied loading induces a more shear-dominant fracture along the grain boundaries, based on the material properties used in the present simulation the specimen will exhibit a more ductile failure behavior and therefore the RVE size will increase.

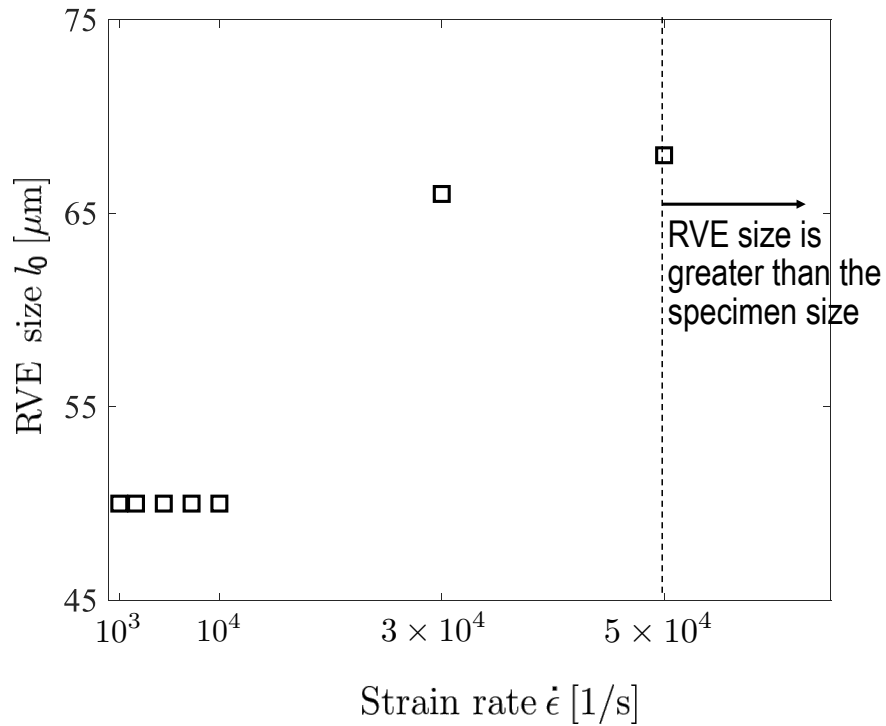


Figure 4.4. Strain rate effect on the RVE size.

Fig. 4.5 presents the influence of the applied strain rate on the strength statistics of the static RVE. We observe that the Weibull modulus increases with the applied strain

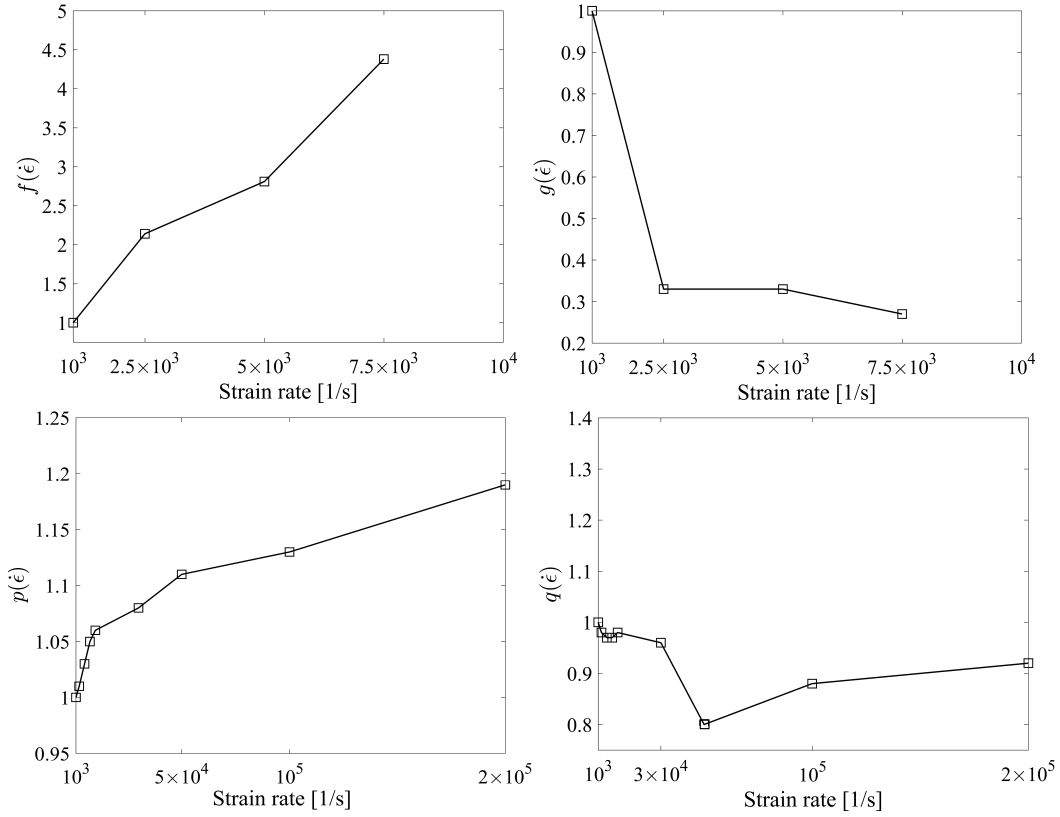


Figure 4.5. Influence of strain rate on the statistical parameters of  $P_1(\sigma_N)$ .

rate (i.e.  $f(\dot{\epsilon}) > 1$  in Eq. 4.5) and the grafting probability decreases with the strain rate (i.e.  $g(\dot{\epsilon}) < 1$  in Eq. 4.6). It is noted that, when the strain rate is higher than 7500/s, the power-law tail of the strength distribution of the static RVE is too short to be determined for the range of the specimen sizes considered here. The observed rate dependence of the strength statistics of static RVE can be attributed to the fact that, as the strain rate increases, the static RVE experiences more dense micro-cracking. In the context of the present stochastic discrete element model, microcracking is represented by the failure of grain boundaries (facets). The increase in the Weibull modulus can be qualitatively explained by a fishnet statistics model, which was recently developed to analyze a fishnet structure for predicting the probability distribution of static strength of nacreous imbricated lamellar materials. Though the specimens dealt in this study are very

different from the fishnet structure, the same mathematical framework can be applied to both cases.

Following the fishnet model [74], the strength distribution of a static RVE can be calculated as

$$F_s(\sigma_N) = 1 - [P_{s,0}(\sigma_N) + P_{s,1}(\sigma_N) + \cdots + P_{s,N}(\sigma_N)] \quad (4.11)$$

where  $P_{s,r}$  = probability that  $r$  number of facets have experienced damage after stress  $\sigma_N$  is applied to the static RVE, and  $N$  = total number of facets. For the practical use of Eq. 4.11, we just need to retain several dominant terms ( $r = 0, \dots, k$ ), which contribute to the overall failure probability. The aforementioned rate effect on microcracking density indicates that  $k$  increases with the applied strain rate. To calculate the individual probability component  $P_{s,r}$  of Eq. 4.11, one would need to determine the load distribution among the facets. A realistic calculation of the load distribution pattern is equivalent to performing the nonlinear stochastic discrete element simulations, which is computationally intensive. Nevertheless, the recent results of the fishnet analysis indicate that, if the strength statistics of each facet has a power-law tail, then the strength distribution of the system will also exhibit a power-law tail. The power-law exponent increases in proportion to the dominant number of damaged facets (i.e.  $k$  in Eq. 4.11) [74]. This explains the observed increase in the Weibull modulus with an increasing strain rate.

The decrease in the grafting probability indicates that the strength distribution of the static RVE approaches a Gaussian distribution. This can be physically related to the observed increasing number of damaged facets, which implies that the failure becomes more ductile. Since more facets contribute to the failure of the static RVE, we expect that the standard deviation would decrease considerably. However, it is also noted that the random mesostructure causes a considerable variability of the stress field, and this variability is further enhanced by the inertia effect. Therefore the stress field becomes more random at high strain rates, which leads to a larger standard deviation of the overall nominal strength. This effect counteracts the aforementioned decrease in the standard deviation due to the increasing number of damaged facets. As shown in Fig. 4.5, the

calibration results show that the overall standard deviation of the strength of static RVE decreases mildly with an increasing strain rate.

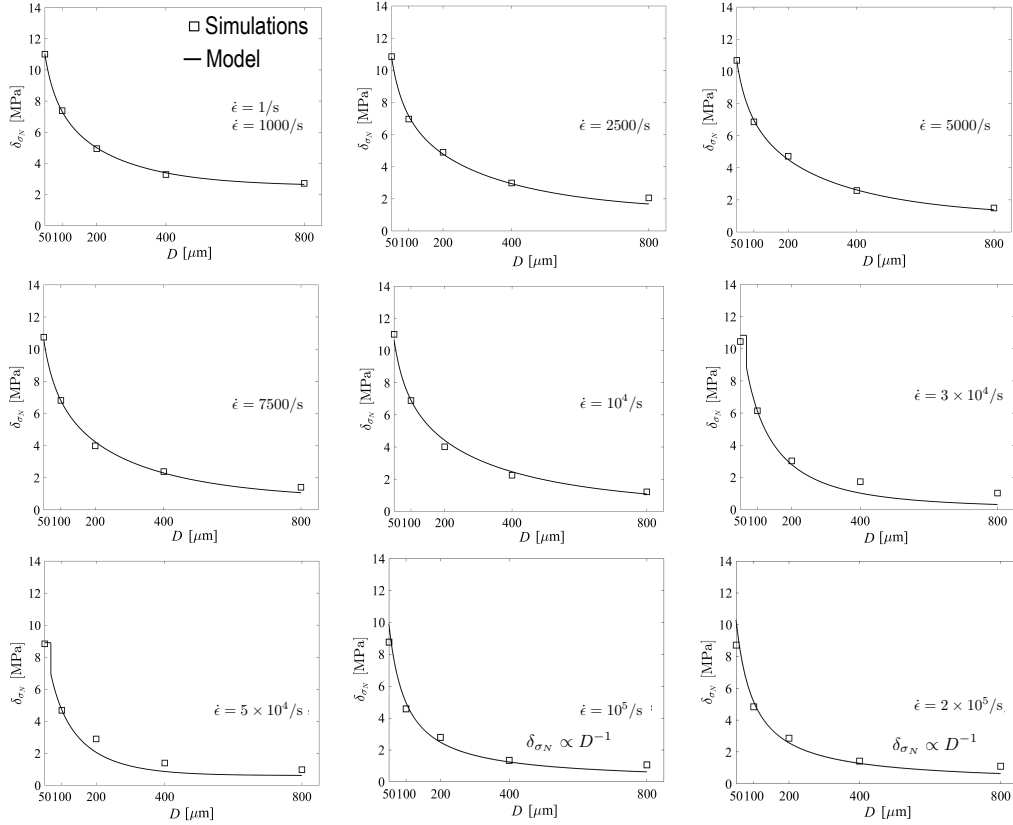


Figure 4.6. Simulated size effects on the standard deviation of nominal strength at different strain rates and its comparison with the rate-dependent finite weakest-link model.

The calibrated rate-dependent weakest-link model is now used to predict the size effect curves of the standard deviation for different applied strain rates. Fig. 4.6 shows that the model prediction agrees well with the simulation results. It is seen that, in contrast to the diminishing size effect on the mean nominal strength at high strain rates, the size effect on the standard deviation becomes more pronounced as the strain rate increases. At low strain rates, the standard deviation exhibits an intricate size effect ending with a power-law asymptote at the large-size limit. This theoretical power-law asymptote is attributed to the fact that, according to the weakest-link model, at low strain rates the

strength distribution of large-size specimens would approach a Weibull distribution, i.e.  $P_f(\sigma_N) = 1 - \exp[-(D/l_0)^2(\sigma_N/s_0)^m]$ . The corresponding standard deviation of  $\sigma_N$  can be written as

$$\delta_{\sigma_N} = s_0 \left(\frac{l_0}{D}\right)^{2/m} \sqrt{\Gamma\left(1 + \frac{2}{m}\right) - \Gamma^2\left(1 + \frac{1}{m}\right)} \quad (4.12)$$

where  $\Gamma(x)$  = Eulerian gamma function. Eq. 4.12 indicates that, at low strain rates, the asymptotic size effect on the standard deviation is very weak since  $m$  is usually a large number.

For the high strain rates considered in this study ( $\dot{\epsilon} > 10^5/\text{s}$ ), the fitting of the mean size effect curve indicates that the specimen size is smaller than the RVE size. According to Eq. 4.3, we have  $n_b = (D/l_{0s})^2$ . Therefore, the statistics of the nominal strength of the specimen is modeled by a plastic bundle, and the scaling of the standard deviation is given by Eq. 4.8. It can be easily shown that, as  $n_b$  increases (i.e.  $n_b > 4$ ), Eq. 4.8 is approximately equivalent to

$$\delta_G(\dot{\epsilon}) = \frac{\delta_{G0}q(\dot{\epsilon})}{\sqrt{n_b}} = \delta_{G0}q(\dot{\epsilon})l_{0s}D^{-1} \quad (4.13)$$

We note that the size effect depicted by Eq. 4.13 is much stronger than that predicted by the Weibull distribution. From Fig. 4.6, we see that Eq. 4.13 agrees well with the simulated size effect on the standard deviation at high strain rates.

The foregoing analysis elucidates the size and rate dependence of the functional form of strength distribution. At low strain rates, the strength distribution of the specimen transitions from a Gaussian distribution modified by a far-left Weibull tail to a Weibull distribution as the specimen size increases. At high strain rates, for the specimens considered in this study, the strength distribution is essentially Gaussian with a constant mean value but a decreasing standard deviation. This transitional behavior is well captured by the present model.

It is also worthwhile to discuss the transition between the low and high strain rates. There could exist a narrow range of intermediate strain rates, where the increase in the RVE size is not significantly large but the grafting probability of the RVE is considerably

reduced (Eq. 4.6). Consider a very large specimen containing a sufficient number of RVEs subjected to such intermediate strain-rate loading. Since the power-law tail of RVE strength becomes very short, for the failure risk of practical interest ( $P_f \approx 10^{-6}$ ), the strength distribution of the specimen can be considered as a long chain of Gaussian elements, which would converge to a Gumbel distribution [44]. Such a Gumbel asymptotic distribution is not seen in the finite weakest-link model for static loading since the Weibull tail is not sufficiently short.

## CHAPTER 5

## Mesh Dependence in Stochastic Simulations of Dynamic Quasibrittle Fracture

### 5.1. Introduction

In this part of the research, we investigate the mesh dependence in stochastic simulations of quasibrittle structures under dynamic loading. Though recent FE simulations of impact resistance of ceramics materials indicated the simulated mean structural response is significantly influenced by the mesh size [20, 69, 108], there is still a lack of understanding of the mesh sensitivity in the simulated statistics of the dynamic response (both first and second statistical moments) of quasibrittle structures.

The split Hopkinson pressure bar (SHPB) test is a widely used experimental tool for assessing the dynamic failure behavior of brittle and quasibrittle materials, such as concrete [95, 60, 102, 109], ceramics [33, 76], and rock [115]. The most well known result of SHPB test is the dynamic increase factor of the material's tensile strength, which has been used in the design of engineering structures under impact loading. In parallel with extensive efforts on experimental investigation, there has also been a strong interest in computational modeling of the SHPB test. Both continuum FE and discrete lattice models have been used to predict the dynamic tensile strength, e.g. [71, 83, 49]. Though previous studies showed the success of these computational models, very few of them have systematically studied the mesh sensitivity in the FE simulations.

The other aspect of the problem that has not received sufficient attention is the statistics of dynamic strength measured by the SHPB test. As mentioned in the problem statement (Chapter 1), understanding the mean structural strength is insufficient for engineering designs since most modern design methodologies are anchored by the concept of structural reliability. At minimum, they require both the mean and standard deviation

of structural strength. However, existing computational modeling of the SHPB test is largely cast in a deterministic form, and therefore the mesh sensitivity issue in stochastic FE simulation of SHPB test has not been investigated.

In this research, we study the dynamic tensile strength of quasibrittle materials measured by the SHPB test. The main focus is to examine the performance of the conventional crack band model and the probabilistic crack band model (Chapter 2). The present analysis shed light on the potential success of a new computational model that combines the probabilistic crack band model and rate-dependent weakest link model.

## 5.2. Description of Analysis

Here we consider a bar specimen with one end subjected to a stress pulse and the other end being free (Fig. 5.1a and b). It is evident that the applied stress pulse will first translate to a compressive stress wave propagating to the right end of the bar. Once the stress wave reaches the free end, it will reflect back as a tensile wave propagating back. By choosing an appropriate input stress pulse with a magnitude smaller than the compressive strength of the material, we can design the experiment so that the bar will fail in tension due to the reflective tensile stress wave, from which we may measure the dynamic tensile strength. In the simulation model, we consider that the specimen has a length of 20 mm and a diameter of 2 mm. Since we are primarily interested in dynamic tensile failure, we adopt a tensile damage constitutive model, which follows the same formulation as what we used for implementing the probabilistic crack band model (i.e. Eqs. 2.16 – 2.18). Here we consider alumina nitride material, which has a mean tensile strength of 220 MPa and a mean fracture energy of 40 N/m.

In the present simulation, we consider three levels of stress pulse ( $\sigma_0 = 450, 675, 900$  MPa,  $t_0 = 5 \times 10^{-6}$ , see Fig. 5.1a), which represent different rates of loading. The nominal strain rate  $\dot{\epsilon}$  is calculated from the applied stress rate:

$$\dot{\epsilon} = 2\sigma_0/Et_0 \quad (5.1)$$

where  $E$  = Young's modulus. The stress pulses considered here correspond to three levels of nominal strain rate ( $\dot{\epsilon} = 500, 750, 1000$ /s).

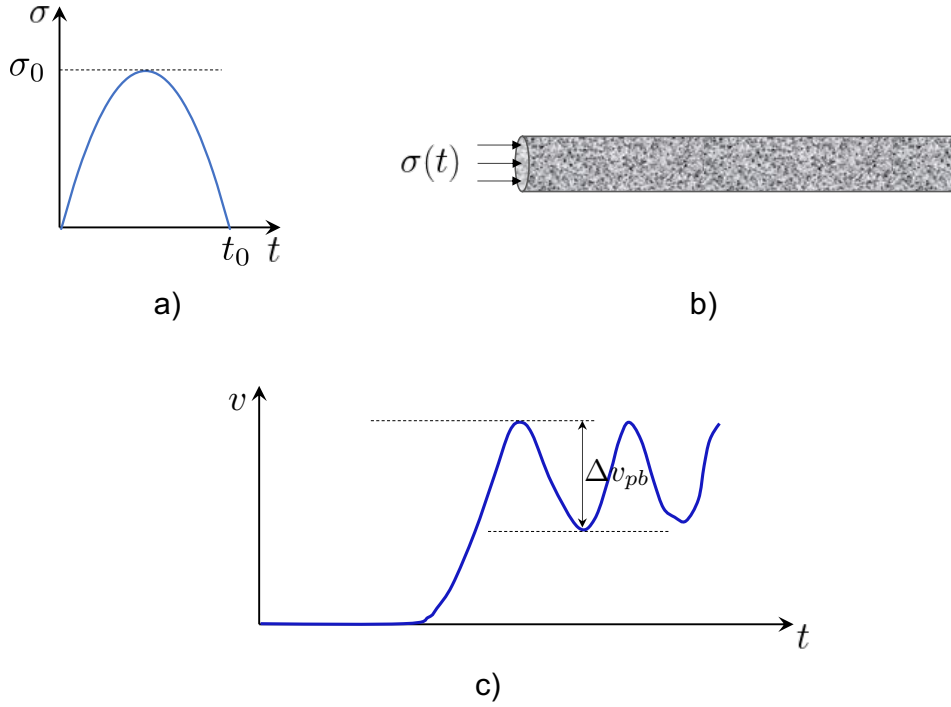


Figure 5.1. Schematics of simulation set-up: a) input stress pulse, b) impacted specimen, and c) a typical free-end velocity profile.

From the simulation, we can calculate the time history of the velocity of the free end. Fig. 5.1c depicts a typical profile of the free end velocity. Following [79, 102, 49], the dynamic tensile strength could be calculated based on the pullback velocity  $\Delta v_{pb}$ , which is defined as the difference between the peak velocity and the rebound velocity, i.e.:

$$\sigma_N = \frac{1}{2} \rho c \Delta v_{pb} \quad (5.2)$$

where  $\rho$  = material density, and  $c = \sqrt{E/\rho}$  = wave velocity. Depending on the input stress pulse, the specimen may experience a single localized crack or multiple crack initiation [49, 90]. Based on the definition of the pullback velocity, the dynamic strength calculated by Eq. 5.2 is related to the first complete cracking of the specimen.

To investigate the issue of mesh sensitivity, we perform a set of stochastic simulations by using the following two approaches:

- Conventional crack band model without considering the mesh dependence of the probability distribution function of material strength,

- Probabilistic crack band model as presented in Chapter 2, which accounts for the mesh dependent probability distribution of material strength as well as the localization parameters.

For each simulation case, we consider three FE mesh sizes ( $h_e = 50, 100, 200\mu\text{m}$ ) along the longitudinal direction, while the other dimensions of the mesh (i.e. along the cross section of the bar) are fixed. The crack band width of the material is taken to be  $20\mu\text{m}$ .

In the simulation, we treat material tensile strength and fracture energy as two independent random variables. When using the conventional crack band model, both tensile strength and fracture energy are considered to follow a Gauss-Weibull distribution, i.e.

$$F(x) = \begin{cases} 1 - \exp[-(x/s_0)^m] \approx (x_{gr}/s_0)^m & (x \leq x_{gr}) \\ P_{gr} + \frac{r_f}{\delta_G \sqrt{2\pi}} \int_{\sigma_{gr}}^x e^{-(x' - \mu_G)^2 / 2\delta_G^2} dx' & (x > x_{gr}) \end{cases} \quad (5.3)$$

in which Weibull modulus  $m = 26$ , grafting probability  $P_{gr} = (x_{gr}/s_0)^m = 10^{-3}$ , and the coefficient of variation (CoV) = 0.15. Since the material strength and fracture energy are independent, there is always a possibility of having a snap-back stress-strain curve. In such a case, we discard this particular sampling of tensile strength and fracture energy. This probability is extremely low for the mesh sizes used in the present study. Furthermore, we assume that the autocorrelation length of the random fields of material strength and fracture energy is similar to the crack band width, which is smaller than the mesh size used in the simulation. Therefore, we may consider that the material strength and fracture energy of each Gauss point of the FE mesh are statistically independent, and the spatial autocorrelation can be ignored. For each simulation case, we perform about 20 to 30 realizations, and calculate the mean and standard deviation of the dynamic tensile strength based on Eq. [5.2](#).

### 5.3. Results and Discussion

Figs. [5.2](#) and [5.3](#) show the simulated mean and standard deviation of the dynamic tensile strength for different mesh sizes and applied stress pulses. It is seen that, compared to the conventional crack band model, the present probabilistic crack band model predicts

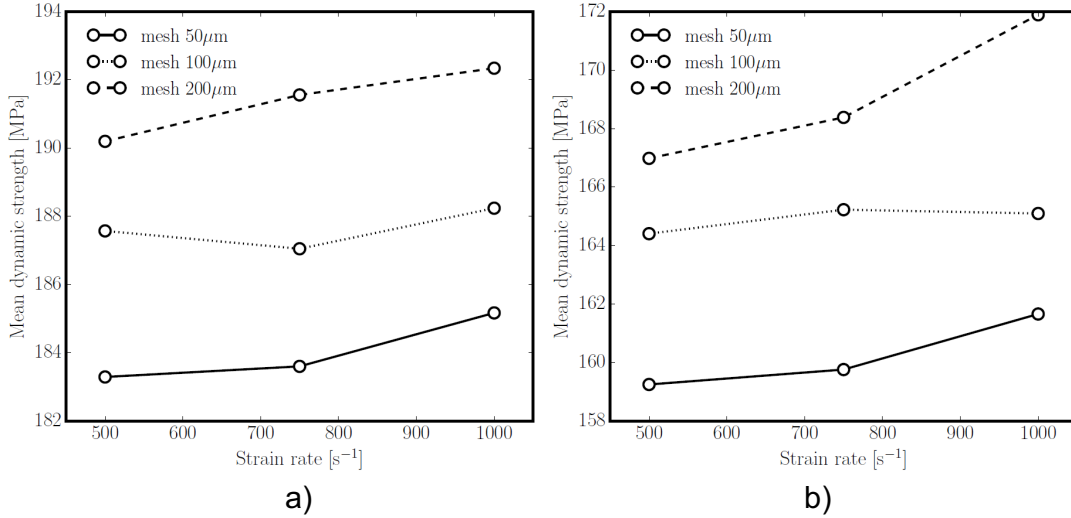


Figure 5.2. Simulated mean dynamic strengths for different mesh sizes: a) conventional crack band model, and b) probabilistic crack band model.

a lower mean strength and higher standard deviation. This is due to the fact that the probabilistic crack band uses the finite weakest-link model for the condition of damage initiation, which predicts a lower mean tensile strength for each Gauss point. This finding implies that, even if we are only interested in the mean response, the result would strongly depend on the choice of the probabilistic model. Furthermore, it is well expected that the mean response simulated by the stochastic simulations would differ from that simulated by the deterministic model even if both models use the same mean inputs. This highlights the important role of stochastic simulations in predicting the structural failure.

By comparing the responses simulated by these two approaches, we can see that, at low rate loading, both of these approaches exhibit a similar and mild level of mesh sensitivity. As the strain rate increases, the level of mesh sensitivity of the conventional crack band model remains almost the same, while the probabilistic crack band model exhibits an increasing level of mesh sensitivity. The underlying reason is that the probabilistic crack band model described in Chapter 2 is anchored by the finite weakest-link model, which does not consider the strain rate effect. Fig. 5.4 shows the simulated damage profile at

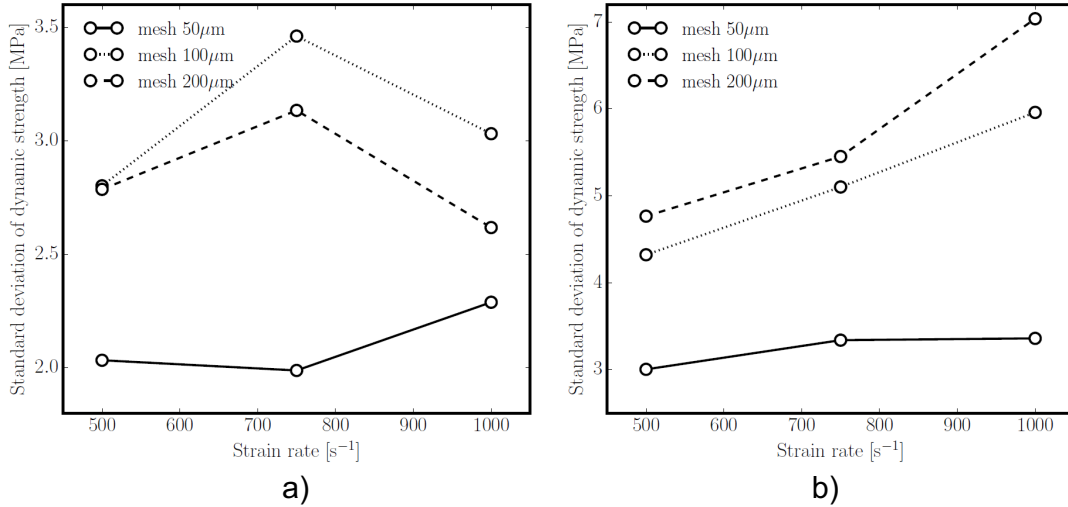


Figure 5.3. Simulated standard deviations of dynamic strength for different mesh sizes: a) conventional crack band model, and b) probabilistic crack band model.

the time when the pullback velocity is recorded. It is clear that, as the applied stress pulse increases (i.e. the nominal applied strain rate increases), the specimen exhibits a more diffused damage. Based on the discussion in Chapter 4, in such a case, the weakest-link model of material strength should gradually transition to a fiber-bundle model, where the functional form of the strength distribution remains the same but the coefficient of variation would decrease with the element size. In the present study, even for the smallest stress pulse, the local strain rate in the element could be sufficiently high, which requires the adjustment of the weakest-link model of material strength.

On the other hand, the conventional crack band model does not involve any adjustment of the probability distribution of material strength. This model is inaccurate for both low and high loading rates. The deficiency of this model at low loading rate has been discussed in Chapter 2. As the loading rate increases, the strength distribution should have a decreasing standard deviation. This is not captured by the conventional crack band model. Another issue of the conventional crack band model is that, as the loading rate

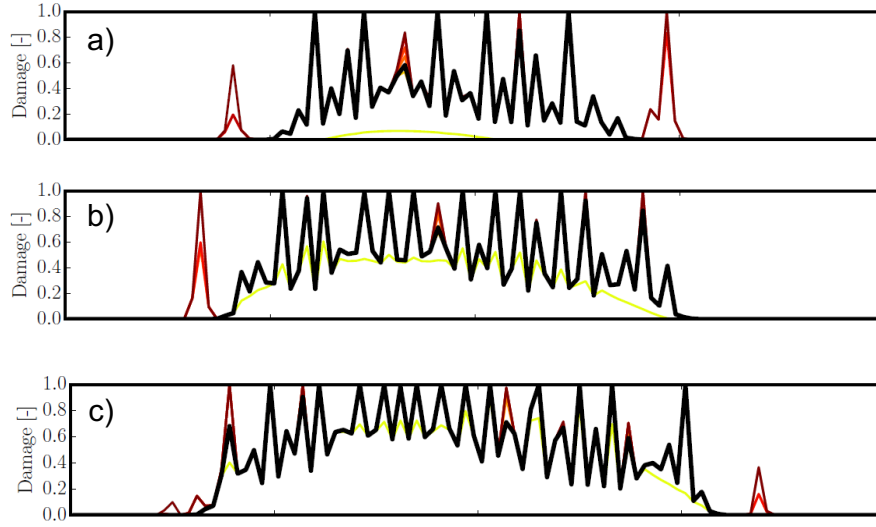


Figure 5.4. Simulated damage profile at the measurement of the pullback velocity: a)  $\dot{\epsilon} = 500/\text{s}$ , b)  $\dot{\epsilon} = 750/\text{s}$ , and c)  $\dot{\epsilon} = 1000/\text{s}$ .

increases, the specimen would exhibit a more diffusive damage pattern instead of localized damage, as shown in Fig. 5.4. In this case, energy regularization becomes unnecessary.

Based on the foregoing discussion, it is evident that neither the conventional crack band model nor the probabilistic crack band model could resolve the mesh sensitivity issue for stochastic simulations of dynamic quasibrittle fracture. Based on Figs. 5.2 and 5.3, we may conclude that the overall performance of the conventional crack band model is slightly better than that of the probabilistic crack band model. This is because, for simulations of dynamic fracture, the weakest-link model used in the probabilistic crack model significantly penalizes the prediction of dynamic strength. By contrast, the conventional crack band model, which uses the same strength distribution, albeit not completely correct, yields a lower level of mesh sensitivity at high loading rates.

It should be pointed out that, compared to the conventional crack band model, the probabilistic crack band model is able to cover more potential failure mechanisms, such as diffusive damage, localized damage, and the transition between them. In order to develop a reliable approach for mitigating the mesh sensitivity issue, we can improve

the probabilistic crack band model by incorporating the rate-dependent finite weakest-link model (Chapter 4). According to the rate-dependent weakest-link model, it is clear that, as the loading rate increases, the statistics of material strength of each Gauss point would approach a Gaussian distribution with a decreasing standard deviation. This will effectively reduce the difference in the simulated standard deviations for different mesh sizes (Fig. 5.3).

Another advantage of using the rate-dependent weakest-link model is that has been calibrated by using a mesoscale stochastic model, as discussed in Chapters 3 and 4. It is clear that the combination of the mesoscale stochastic model and the present probabilistic crack band model has led to a multiscale computational framework for stochastic computation of quasibrittle fracture under static loading. This framework can easily be extended to dynamic fracture by incorporating the calibrated rate-dependent weakest-link model into the probabilistic crack band model. Such a multiscale computational framework would faithfully capture the effect of the probabilistic failure behavior at the mesoscale on the failure statistics of macroscopic structures.

## CHAPTER 6

# Conclusions and Future Work

### 6.1. Conclusions

1. The conventional crack band model is insufficient for resolving the issue of mesh dependence in stochastic simulations of quasibrittle structures. The underlying reason for such mesh dependence lies in the lack of consideration of the random onset of localization band inside the material element. The mesh dependence of stochastic FE simulations of quasibrittle fracture can effectively be mitigated by using a finite weakest link model for the randomness of the damage localization band in each material element. The statistics of the random onset of localization is governed by the localization level of its neighboring elements.

2. The strain rate has a profound influence on the scaling of the nominal tensile strength of quasibrittle structures. This rate dependence arises from the effect of the strain rate on the failure behavior of the structure. The discrete element simulations show that the structure exhibits a more diffused cracking pattern as the strain rate increases, which explains the observed diminishing mean size effect at high strain rates. Meanwhile, the rate-dependent failure behavior also leads to different scaling behaviors of the standard deviation of the nominal strength at different strain rates. It is shown that, for a given strain rate, the standard deviation decreases with an increasing specimen size. At high strain rates, this decreasing trend becomes stronger and it exhibits a power-law scaling behavior. The result also indicates that, for a given specimen size, an increasing strain rate leads to a reduction in the standard deviation of the nominal strength.

3. The simulated rate and size effects on the mean and standard deviation of the nominal tensile strength can be well captured by a rate-dependent finite weakest link model. The model employs a rate-dependent length scale, which physically represents

the transition from damage localization to diffused damage with an increasing strain rate. The model directly predicts the combined rate and size effects on the probability distribution of the nominal strength. At low strain rates, the strength distribution varies from a predominant Gaussian distribution to a Weibull distribution as the specimen size increases, while at high strain rates, the strength distribution is Gaussian for a large range of specimen sizes. The present rate-dependent finite weakest link model provides an analytical tool to model the rate and size effects on the probability distribution of nominal tensile strength, which could be implemented into the stochastic FE simulation of dynamic fracture of quasibrittle structures.

4. The present stochastic simulations of the split Hopkinson pressure bar experiment show that the predicted mean dynamic tensile strength is strongly dependent on the choice of the probabilistic model. This indicates that the response predicted by a deterministic model would differ from the mean response predicted by a stochastic model, which implies the importance of stochastic modeling of material failure. Meanwhile, it is seen that neither the conventional crack band model nor the probabilistic crack band model described in Chapter 2 could resolve the mesh sensitivity issue satisfactorily. However, the simulation trend indicates that the combination of the probabilistic crack band model and the rate-dependent weakest-link model would provide an effective multiscale computational framework for mitigating the mesh dependence issue in stochastic simulation of dynamic quasibrittle fracture.

## 6.2. Future Work

1. The recently developed probabilistic crack band model and the rate-dependent weakest model can now be combined to form a new mesh regularization approach for stochastic simulation of quasibrittle fracture under dynamic loading. The last part of the study shows the promise of this new approach. While the present study focuses on tensile damage, the model can be incorporated into some established material constitutive models for predicting more complicated dynamic failure behavior of different quasibrittle structures.

2. The present study considers the case where the mesh size is larger than the crack band width. By further considering that autocorrelation length of the random material properties is similar to the crack band width, we ignore the autocorrelation feature of the random field. It is interesting to extend the model to the case of small mesh size. For such an extension, we will need to consider explicitly the full information of the random field of material properties including its autocorrelation features. The fundamental question is how to project the generated random field onto the Gauss point of each FE mesh. Existing approaches for this projection largely rely on either local mapping or local averaging, neither of which is linked with the underlying failure mechanism. Therefore, it is necessary to develop a new mechanics-based method for relating the random field to the probability distribution of the constitutive properties of the FE Gauss point. It is foreseen that this approach will be a generalization of the present probabilistic crack band model.

## References

- [1] E. C. Aifantis. On the microstructural origin of certain inelastic models. *J. Eng. Mater. Tech., ASME*, 106:326–330, 1984.
- [2] S. Esna Ashari, G. Buscarnera, and G. Cusatis. A lattice discrete particle model for pressure-dependent inelasticity in granular rocks. *International Journal of Rock Mechanics and Mining Sciences*, 91:49–58, 2017.
- [3] M. F. Ashby and C. G. Sammis. The damage mechanics of brittle solids in compression. *PAGEOPH*, 133:489–521, 1990.
- [4] K.-J. Bathe. *Finite element procedures*. Prentice Hall, Englewood Cliffs, N.J., 1996.
- [5] Z. P. Bažant. Imbricate continuum and progressive fracturing of concrete and geomaterials. *Meccanica*, 19:86–93, 1984.
- [6] Z. P. Bažant. Mechanics of fracture and progressive cracking in concrete structures. In G. C. Sih and A. DiTommaso, editors, *Fracture Mechanics of Concrete: Structural Application and Numerical Calculation*, pages 1–94, Dordrecht and Boston, 1985. Martinus Nijhoff.
- [7] Z. P. Bažant. *Scaling of Structural Strength*. Elsevier, London, 2005.
- [8] Z. P. Bažant and M. Jirásek. Nonlocal integral formulations of plasticity and damage: Survey of progress. *J. Engrg. Mech., ASCE*, 128(11):1119–1149, 2002.
- [9] Z. P. Bažant and J.-L. Le. *Probabilistic Mechanics of Quasibrittle Structures: Strength, Lifetime, and Size Effect*. Cambridge University Press, Cambridge, U.K., 2017.
- [10] Z. P. Bažant, J.-L. Le, and M. Z. Bazant. Scaling of strength and lifetime distributions of quasibrittle structures based on atomistic fracture mechanics. *Proc. Nat'l. Acad. Sci., USA*, 106:11484–11489, 2009.

- [11] Z. P. Bažant and B. H. Oh. Crack band theory for fracture of concrete. *Mater. Struct.*, 16:155–177, 1983.
- [12] Z. P. Bažant and S. D. Pang. Activation energy based extreme value statistics and size effect in brittle and quasibrittle fracture. *J. Mech. Phys. Solids.*, 55:91–134, 2007.
- [13] Z. P. Bažant and G. Pijaudier-Cabot. Nonlocal continuum damage, localization instability and convergence. *J. App. Mech., ASME*, 55:287–293, 1988.
- [14] Z. P. Bažant and J. Planas. *Fracture and Size Effect in Concrete and Other Quasibrittle Materials*. CRC Press, Boca Raton and London, 1998.
- [15] Z. P. Bažant, M. R. Tabbara, M. T. Kazemi, and G. Pijaudier-Cabot. Random particle model for fracture of aggregate or fiber composites. *J. Engrg. Mech., ASCE*, 116(8):1686–1705, 1990.
- [16] H. S. Bhat, A. J. Rosakis, and C. G. Sammis. A micromechanics based constitutive model for brittle failure at high strain rates. *J. Appl. Mech. ASME*, 79(3):031016, 2012.
- [17] W. R. Blumenthal. High strain rate compression testing of ceramics and ceramic composites. In J. J. Swab, editor, *Advances in Ceramic Armor. Ceram Eng. Sci. Proc.*, volume 26, pages 89–96, 2005.
- [18] J. E. Bolander, G. S. Hong, and K. Yoshitake. Structural concrete analysis using rigid-body-spring networks. *J. Comput. Aided Civil Infrastruct. Eng.*, 15:120–133, 2000.
- [19] J. E. Bolander and S. Saito. Fracture analysis using spring network with random geometry. *Engrg. Fract. Mech.*, 61(5-6):569–591, 1998.
- [20] R. M. Brannon, J. M. Wells, and O. E. Strack. Validating theories for brittle damage. *Metallurgical Mater. Trans. A.*, 38(A):2861–2868, 2007.
- [21] J. D. Clayton, R. H. Kraft, and R. B. Leavy. Mesoscale modeling of nonlinear elasticity and fracture in ceramics polycrystals under dynamic shear and compression. *Int. J. Solids Struct.*, 49:2686 – 2702, 2012.
- [22] P. A. Cundall. A computer model for simulating progressive large scale movements in blocky rock systems. In *Proc. Int. Symp. Rock Fracture*, volume 1, pages Paper No. II–8, Nancy, France, 1971.

- [23] P. A. Cundall and O. Strack. A discrete numerical model for granular assemblies. *Geotechnique*, 29(1):47–65, 1979.
- [24] G. Cusatis. Strain-rate effect on concrete behavior. *Int. J. Impact Engrg.*, 38(4):162–170, 2011.
- [25] G. Cusatis, Z. P. Bažant, and L. Cedolin. Confinement-shear lattice model for concrete damage in tension and compression: I. theory. *J. Engrg. Mech., ASCE*, 129(12):1439–1448, 2003.
- [26] G. Cusatis, Z. P. Bažant, and L. Cedolin. Confinement-shear lattice model for concrete damage in tension and compression: I. Theory. *J. Engrg. Mech., ASCE*, 129(12):1439–1448, 2003.
- [27] G. Cusatis, Z. P. Bažant, and L. Cedolin. Confinement-shear lattice model for concrete damage in tension and compression: II. Computation and validation. *J. Engrg. Mech., ASCE*, 129(12):1449–1458, 2003.
- [28] G. Cusatis and L. Cedolin. Two-scale study of concrete fracturing behavior. *Engineering Fracture Mechanics*, 74(1):3–17, 2007. Fracture of Concrete Materials and Structures.
- [29] G. Cusatis, A. Mencarelli, D. Pelessone, and J. Baylot. Lattice discrete particle model (LDPM) for failure behavior of concrete. II: Calibration and validation. *Cement and Concrete Composites*, 33(9):891–905, 2011.
- [30] G. Cusatis, D. Pelessone, and A. Mencarelli. Lattice discrete particle model (LDPM) for failure behavior of concrete. I. Theory. *Cem. Concr. Comp.*, 22:881–890, 2011.
- [31] H. E. Daniels. The statistical theory of the strength of bundles and threads. *Proc. R. Soc. London A.*, 183:405–435, 1945.
- [32] N. P. Daphalapurkar, K.T. Ramesh, L. Graham-Brady, and J.-F. Molinari. Predicting variability in the dynamic failure strength of brittle materials considering pre-existing flaws. *J. Mech. Phys. Solids*, 59:297–319, 2011.
- [33] F. Gálvez Díaz-Rubio, J. Rodríguez Pérez, and V. Sánchez Gálvez. The spalling of long bars as a reliable method of measuring the dynamic tensile strength of ceramics. *Int. J. Impact Engrg.*, 27(2):161–177, 2002.
- [34] J. Eliáš. Adaptive technique for discrete models of fracture. *International Journal of Solids and Structures*, 100-101:376–387, 2016.

- [35] J. Eliáš, M. Vořechovský, J. Skoček, and Z. P. Bažant. Stochastic discrete meso-scale simulations of concrete fracture: Comparison to experimental data. *Engrg. Fract. Mech.*, 135(1):1–16, 2015.
- [36] H. D. Espinosa, P. D. Zavattieri, and S. Dwivedi. A finite deformation continuum discrete model for the description of fragmentation and damage in brittle materials. *J. Mech. Phys. Solids*, 46:1909–1942, 1998.
- [37] R. A. Fisher and L. H. C. Tippett. Limiting form of the frequency distribution the largest and smallest number of a sample. *Proc. Cambridge. Philos. Soc.*, 24:180–190, 1928.
- [38] M. Fréchet. Sur la loi de probabilité de l' écart maximum. *Ann. Soc. Polon. Math. (Cracow)*, 6:93, 1927.
- [39] F. Gatuingt, L. Snozzi, and J. F. Molinari. Numerical determination of the tensile response and the dissipated fracture energy of concrete: role of the mesostructure and influence of the loading rate. *Int. J. for Numer. and Anal. Methods in Geomech.*, 37:3112–3130, 2013.
- [40] R. Ghanem and P. D. Spanos. *Stochastic Finite Elements: A Spectral Approach*. Dover Publications, New York, 2nd ed. edition, 2003.
- [41] L. Graham-Brady. Statistical characterization of meso-scale uniaxial compressive strength in brittle materials with randomly occurring flaws. *Int. J. Solids Struct.*, 47:2398–2413, 2010.
- [42] P. Grassl and Z. P. Bažant. Random lattice-particle simulation of statistical size effect in quasibrittle structures failing at crack initiation. *J. Eng. Mech., ASCE*, 135(2):85–92, 2009.
- [43] D.L. Grote, S.W. Park, and M. Zhou. Dynamic behavior of concrete at high strain rates and pressures: I. experimental characterization. *Int. J. Impact Engrg.*, 25:869–886, 2001.
- [44] E. J. Gumbel. *Statistics of Extremes*. Columbia University Press, New York, 1958.
- [45] Z. Hashin. Analysis of composite materials - A survey. *J. Appl. Mech. ASME*, 50:481–505, 1983.
- [46] R. Hill. A general theory of uniqueness and stability in elastic-plastic solids. *J. Mech. Phys. Solids*, 6:236–249, 1958.

- [47] R. Hill. Elastic properties of reinforced solids: some theoretical principles. *J. Mech. Phys. Solids*, 11:357–362, 1963.
- [48] A. Hrennikoff. Solution of problems of elasticity by the framework method. *J. Appl. Mech.*, 12:169–175, 1941.
- [49] Y. K. Hwang, J. E. Bolander, and Y. M. Lim. Simulation of concrete tensile failure under high loading rates using three-dimensional irregular lattice models. *Mech. Mater.*, 101:136–146, 2016.
- [50] Y. K. Hwang and Y. M. Lim. Validation of three-dimensional irregular lattice model for concrete failure mode simulations under impact loads. *Engrg. Frac. Mech.*, 169:109–127, 2017.
- [51] K. Iwashita and M. Oda. *Mechanics of Granular Materials: An Introduction*. CRC press, Boca Raton, FL, USA, 1999.
- [52] M. Jirásek. Mathematical analysis of strain localization. *Revue Européenne de Génie Civil*, 11:977–991, 2007.
- [53] M. Jirásek and M. Bauer. Numerical aspects of the crack band approach. *Comp. Struct.*, 110-111:60–78, 2012.
- [54] M. Jirásek and Z. P. Bažant. Macroscopic fracture characteristics of random particle systems. *Int. J. Frac.*, 69:201–228, 1995.
- [55] M. Jirásek and Z. P. Bažant. Particle model for quasibrittle fracture and application to sea ice. *J. Engrg. Mech. ASCE*, 121:1016–1025, 1995.
- [56] M. Jirásek and Z. P. Bažant. *Inelastic Analysis of Structures*. Wiley, Chichester, 2002.
- [57] A. Kara, A. Tasdemirci, and M. Guden. Modeling quasi-static and high strain rate deformation and failure behavior of a ( $\pm 45$ ) symmetric e-glass/polyester composite under compressive loading. *Mater. Des.*, 49:566–574, 2013.
- [58] T. Kawai. New discrete element models and their application to seismic response analysis of structures. *Nucl. Eng. Des.*, 48:207–229, 1978.
- [59] J. Kimberley, K. T. Ramesh, and N. P. Daphalapurkar. A scaling law for the dynamic strength of brittle solids. *Acta Materialia*, 61:3509–3521, 2013.

- [60] J. R. Klepaczko and A. Brara. An experimental method for dynamic tensile testing of concrete by spalling. *Int. J. Impact Engrg.*, 25(4):387–409, 2001.
- [61] R. H. Kraft, J. F. Molinari, K. T. Ramesh, and D. H. Warner. Computational micromechanics of dynamic compressive loading of a brittle polycrystalline material using a distribution of grain boundary properties. *J. Mech. Phys. Solids*, 56:2618–2641, 2008.
- [62] J. Lankford. High strain rate compression and plastic flow of ceramics. *J. Mater. Sci. Lett*, 15:745–750, 1996.
- [63] J.-L. Le and Z. P. Bažant. Unified nano-mechanics based probabilistic theory of quasibrittle and brittle structures: II. Fatigue crack growth, lifetime and scaling. *J. Mech. Phys. Solids.*, 59:1322–1337, 2011.
- [64] J.-L. Le, Z. P. Bažant, and M. Z. Bazant. Unified nano-mechanics based probabilistic theory of quasibrittle and brittle structures: I. strength, crack growth, lifetime and scaling. *J. Mech. Phys. Solids*, 59:1291–1321, 2011.
- [65] J.-L. Le, A. Cannone Falchetto, and M. O. Marasteanu. Determination of strength distribution of quasibrittle structures from mean size effect analysis. *Mech. Mater.*, 66:79–87, 2013.
- [66] J.-L. Le and J. Eliáš. A probabilistic crack band model for quasibrittle fracture. *J. Appl. Mech. ASME*, 83(5):051005, 2016.
- [67] J.-L. Le, Z. Xu, and J. Eliáš. Internal length scale of weakest-link statistical model for quasibrittle fracture. *J. Eng. Mech., ASCE*, (DOI: 10.1061/(ASCE)EM.1943-7889.0001430), 2017.
- [68] J.-L. Le and B. Xue. Energetic-statistical size effect in fracture of bimaterial hybrid structures. *Eng. Frac. Mech.*, 111:106–115, 2013.
- [69] R. B. Leavy, R. M. Brannon, and O. E. Strack. The use of sphere indentation experiments to characterize ceramic damage models. *Int. J. Appl. Cer. Tech.*, 7(5):606–615, 2007.
- [70] C.-C. Li and A. Der Kiureghian. Optimal discretization of random fields. *J. Engrg. Mech., ASCE*, 119(6):1136–1154, 1993.
- [71] Q. M. Li and H. Meng. About the dynamic strength enhancement of concrete-like materials in a split hopkinson pressure bar test. *Int. J. Solids Struct.*, 40:343–360, 2003.

- [72] Z. Li and J. Lambros. Determination of the dynamic response of brittle composites by the use of the split Hopkinson pressure bar. *Comp. Sci. Tech.*, 59:1097–1107, 1999.
- [73] G. Liliu and J. G. M. van Mier. 3D lattice type fracture model for concrete. *Engrg. Fract. Mech.*, 70:927–941, 2003.
- [74] W. Luo and Z. P. Bažant. Fishnet statistics for probabilistic strength and scaling of nacreous imbricated lamellar materials. *J. Mech. Phys. Solids*, 109:264–287, 2017.
- [75] Jacky Mazars. *Application de la mécanique de l'endommagement au comportement non linéaire et à la rupture du béton de structure*. PhD thesis, Univ. Paris VI, Paris, France, 1984.
- [76] J. W. McCauley and G. D. Quinn. Special workshop: Kolsky/split hopkinson pressure bar testing of ceramics. Technical report, U.S. Army Research Laboratory, 2006.
- [77] S. Nemat-Nasser and H. Deng. Strain-rate effect on brittle failure in compression. *Acta Metall. Mater.*, 42(3):1013–1024, 1994.
- [78] N. Newmark. *A method of computation for structural dynamics*. University of Illinois, Urbana, 1959.
- [79] S. A. Novikov, I. I. Divnov, and A. G. Ivanov. The study of fracture of steel, aluminium and copper under explosive loading. *Fizika Metallov i Metallovedeniye*, 21(4):608–615, 1966.
- [80] N. Ottosen and K. Runesson. Properties of discontinuous bifurcation solutions in elasto-plasticity. *Int. J. Solids Struct.*, 27:401–421, 1991.
- [81] J. Ožbolt, J. Bošnjak, and E. Sola. Dynamic fracture of concrete compact tension specimen: Experimental and numerical study. *Int. J. Solids Struct.*, 50(25):4270–4278, 2013.
- [82] J. Ožbolt, A. Sharma, and H.-W. Reinhardt. Dynamic fracture of concrete – compact tension specimen. *Int. J. Solids Struct.*, 48(10):1534–1543, 2011.
- [83] J. Ožbolt, J. Weerheijm, and A. Sharma. Dynamic tensile resistance of concrete – Split Hopkinson bar test. In J.G.M. Van Mier, G. Ruiz, C. Andrade, R. C. Yu, and X. X. Zhang, editors, *VIII International Conference on Fracture Mechanics of Concrete and Concrete Structures (FraMCoS-8)*, pages 1–12, 2013.

- [84] B. Paliwal and K. T. Ramesh. An interacting micro-crack damage model for failure of brittle materials under compression. *J. Mech. Phys. Solids*, 56(3):896–923, 2008.
- [85] B. Patzák and D. Rypl. Object-oriented, parallel finite element framework with dynamic load balancing. *Advances in Engineering Software*, 47:35–50, 2012.
- [86] Bořek Patzák. OOFEM - an object-oriented simulation tool for advanced modeling of materials and structures. *Acta Polytechnica*, 52:59–66, 2012.
- [87] R. H. J. Peerings, M. G. D. Geers, R. de Borst, and W. A. M. Brekelmans. A critical comparison of nonlocal and gradient-enhanced softening continua. *Int. J. Solids Struct.*, 38:7723–7746, 2001.
- [88] R. H. J. Peerlings, R. de Borst, W. A. M. Brekelmans, and J. H. P. de Vree. Gradient-enhanced damage for quasi-brittle materials. *Int. J. Numer. Methods in Eng.*, 39:3391–3403, 1996.
- [89] R.H.J. Peerlings, R. de Borst, W.A.M. Brekelmans, and J.H.P. De Vree. Gradient enhanced damage for quasi-brittle materials. *Int. J. Numer. Methods in Engrg.*, 39:3391–3403, 1996.
- [90] L. F. Pereira, J. Weerheijm, and L.J. Sluys. A new effective rate dependent damage model for dynamic tensile failure of concrete. *Engrg. Frac. Mech.*, 176:281–299, 2017.
- [91] S. L. Phoenix. Stochastic strength and fatigue of fiber bundles. *Int. J. Frac.*, 14(3):327–344, 1978.
- [92] S. L. Phoenix and L.-J. Tierney. A statistical model for the time dependent failure of unidirectional composite materials under local elastic load-sharing among fibers. *Engrg. Fract. Mech.*, 18(1):193–215, 1983.
- [93] G. Pijaudier-Cabot and Z. P. Bažant. Nonlocal damage theory. *J. Engrg. Mech. ASCE*, 113(10):1512–1533, 1987.
- [94] E. Rizzi, I. Carol, and K. Willam. Localization analysis of elastic degradation with application to scalar damage. *J. Eng. Mech., ASCE*, 121:541–554, 1996.
- [95] C. A. Ross, P. Y. Thompson, and J. W. Tedesco. Split-hopkinson pressure-bar tests on concrete and mortar in tension and compression. *ACI Mater. J.*, 86(5):475–481, 1989.
- [96] L. Rothenburg and R. J. Bathurst. Analytical study of induced anisotropy in idealized granular materials. *Geotechnique*, 39(4):601–614, 1989.

- [97] J. W. Rudnicki and J. R. Rice. A conditions for the localization of deformation in pressure-sensitive dilatant materials. *J. Mech. Phys. Solids*, 23:371–394, 1976.
- [98] M. Salviato and Z. P. Bažant. The asymptotic stochastic strength of bundles of elements exhibiting general stress-strain laws. *Prob. Engrg. Mech.*, 36:1–7, 2014.
- [99] E. A. Schaufert and G. Cusatis. Lattice discrete particle model for fiber-reinforced concrete. I: Theory. *J. Engrg. Mech. ASCE*, 138(7):826–833, 2011.
- [100] E. A. Schaufert, G. Cusatis, D. Pelessone, J. L. O’Daniel, and J. T. Baylot. Lattice discrete particle model for fiber-reinforced concrete. II: Tensile fracture and multiaxial loading behavior. *J. Engrg. Mech. ASCE*, 138(7):834–841, 2011.
- [101] E. Schlangen and J. G. M. van Mier. Experimental and numerical analysis of micromechanisms of fracture of cement-based composites. *Cem. Concr. Res.*, 14:105–118, 1992.
- [102] H. Schuler, C. Mayrhofer, and K. Thoma. Spall experiments for the measurement of the tensile strength and fracture energy of concrete at high strain rates. *Int. J. Impact Engrg.*, 32(10):1635–1650, 2006.
- [103] M. Shinozuka and G. Deodatis. Simulation of stochastic processes by spectral representation. *Appl. Mech. Rev. (ASME)*, 44:191–203, 1991.
- [104] J. Smith and G. Cusatis. Numerical analysis of projectile penetration and perforation of plain and fiber reinforced concrete slabs. *Int. J. for Numer. and Anal. Methods in Geomech.*, 41(3):315–337, 2017.
- [105] J. Smith, G. Cusatis, D. Pelessone, E. Landis, J. L. O’Daniel, and J. Baylot. Discrete modeling of ultra-high-performance concrete with application to projectile penetration. *Int. J. Impact Engrg.*, 65:13–32, 2014.
- [106] G. Stefanou. The stochastic finite element method: Past, present and future. *Comput. Methods Appl. Mech. Engrg.*, 198:1031–1051, 2009.
- [107] F. Tonon. Explicit exact formulas for the 3-D tetrahedron inertia tensor in terms of its vertex coordinates. *J. Math. Stat.*, 1(1):8–11, 2005.
- [108] Meyer Jr. H. W. and R. M. Brannon. A model for statistical variation of fracture properties in a continuum mechanics code. *Int. J. Impact Engrg.*, 42:48–58, 2012.

- [109] J. Weerheijm and J.C.A.M. Van Doormaal. Tensile failure of concrete at high loading rates: new test data on strength and fracture energy from instrumented spalling tests. *Int. J. Impact Engrg.*, 34:609–626, 2007.
- [110] J. Weerheijm, I. Vegt, and K. van Breugel. Research developments and experimental data on dynamic concrete behaviour. In *Conference on Advances in Construction Materials*, pages 765–773, Stuttgart, Germany, 2007.
- [111] W. Weibull. The phenomenon of rupture in solids. *Proc. Royal Sweden Inst. Engrg. Res.*, 153:1–55, 1939.
- [112] W. Weibull. A statistical distribution function of wide applicability. *J. Appl. Mech. ASME*, 153(18):293–297, 1951.
- [113] P. D. Zavattieri, P. V. Raghuram, and H. D. Espinosa. A computational model of ceramic microstructures subjected to multi-axial dynamic loading. *J. Mech. Phys. Solids*, 49:27–68, 2001.
- [114] F. Zhou and J. F. Molinari. Stochastic fracture of ceramics under dynamic tensile loading. *Int. J. Solids Struct.*, 41:6573–6596, 2004.
- [115] W. C. Zhu, Y. Bai, X. B. Li, and L. L. Niu. Numerical simulation on rock failure under combined static and dynamic loading during shpb tests. *Int. J. Impact Engrg.*, 49:142–157, 2012.
- [116] A. Zubelewicz and Z. P. Bažant. Interface modeling of fracture in aggregate composites. *J. Engrg. Mech., ASCE*, 113(11):1619–1630, 1987.